RICE UNIVERSITY

Time-Varying Stability Analysis of Linear Systems with Linear Matrix Inequalities
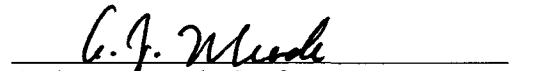
by

John Wilder

A THESIS SUBMITTED
IN PARTIAL FULFILLMENT OF THE
REQUIREMENTS FOR THE DEGREE

Master of Science

APPROVED, THESIS COMMITTEE:

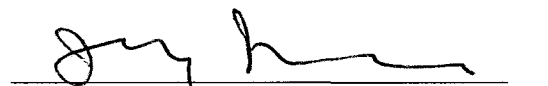Pol D. Spanos, Professor, L. B. Ryon
Chair in Engineering

Andrew J. Meade, Professor
Mechanical Engineering & Materials Science

Ilinca Stanciulescu, Assistant Professor
Civil & Environmental Engineering

Jiann-Woei Jang, Technical Supervisor
Principle Member of the Technical Staff
The Charles Stark Draper Laboratory

HOUSTON, TEXAS
MAY, 2010

UMI Number: 1486044

UMI®

Dissertation Publishing

ProQuest®

ABSTRACT

Time-Varying Stability Analysis of Linear Systems with Linear Matrix Inequalities

by

John Wilder

Aerospace attitude control systems are often modeled as time-varying linear systems. In industry, these systems are analyzed with linear time-invariant (LTI) methods by treating the system as slowly varying. Stability analysis with parameter dependent Lyapunov functions and linear matrix inequalities (LMIs) enables the consideration of bounds on system parameters' rates of variation while accounting for time-varying behavior. The LMI criteria are adapted to predict robustness in time-varying systems. In a case study, stability envelopes are created for time-varying uncertain parameters in a spacecraft. The time-of-flight is divided into intervals and analyzed using typical trajectories of time-varying parameters. For the uncertain parameter combinations considered, LMI stability criteria deduce that the system is stable and possesses stability margins that meet or exceed requirements for the time intervals that can be approximated by linear system models.

Acknowledgments

I want to acknowledge and thank several individuals for supporting my research and thesis-writing efforts throughout my stay in Houston. First, I thank my parents, brother, and the rest of my family for their unconditional love and support of my endeavors. I am very grateful to my advisor, Dr. Spanos, for giving direction to my research and providing endless council and learning opportunities during my time at Rice. Further, I must thank my supervisor, Dr. Jang, for patiently providing invaluable advice, insight, and assistance from an experienced perspective. I also acknowledge and thank Dr. Bedrossian and Draper Laboratory for challenging me and sponsoring my research. I must extend thanks to all my fellow Draper students for their assistance and support over the last two years and for turning the office into a more enjoyable work environment than I could ever hope to find again. Finally, thank you to my girlfriend, my roommates, and all the people in Houston who have made these past 20 months very special in and out of the classroom.

Contents

List of Figures

List of Tables

List of Variables and Abbreviations

$Co\{.\}$ = denotes a convex set

CLV = crew launch vehicle

LFT = linear fractional transformation

LMI = linear matrix inequality

LTI = linear time-invariant

PDS = parameter dependent system

$\phi_{c.g.}$ = vehicle pitch angle about the center of gravity (rad)

α = angle of attack (rad)

β_{CMD} = engine gimbal angle (rad)

β_E = engine gimbal command angle (rad)

$Z_{c.g.}$ = displacement of vehicle c.g. normal to reference (m)

Z_{sj} = sloshing fluid displacement of ith tank (m)

m_{sj} = slosh mass in j^{th} tank (m)

l_{sj} = c.g.-to-slosh-mass distance (m)

M = total vehicle mass (kg)

c_1 = $\frac{C_{Z\alpha}qA(X_{c.g.}-X_{c.p.})}{I_{xx}}$ is an aerodynamic acceleration coefficient (1/sec^2)

c_2 = $R'X_{c.g.}/I_{xx}$ is vehicle angular acceleration (rad/sec^2)

I_{xx} = pitch-yaw vehicle moment of inertia (kg m^2)

$X_{c.g.}$ = center of gravity measured from the gimbal (m)

$X_{c.p.}$ = center of pressure measured from the gimbal (m)

S_E = engine 1st moment about gimbal (kg m)

I_E = engine 2nd moment about gimbal (kg m^2)

k_3 = $(F - D)/M$ vehicle acceleration (m/sec^2)

k_4 = R'/M acceleration due to gimballing (m/sec^2)

k_7 = $C_{Z\alpha}qA/M$ acceleration due to aerodynamic forces (m/sec^2)

$C_{Z\alpha}$ = rigid-body aerodynamic side force coefficient slope (unitless)

q = dynamic pressure (N/m^2)

A = reference area (m^2)

R' = gimbaled engine thrust (N)

V_w = cross-wind velocity (m/sec)

V = vehicle velocity (m/sec)

z_{bi} = damping factor of the ith bending mode (unitless)

ω_{bi} = natural frequency of the ith bending mode (rad/sec)

M_i = generalized mass of the ith bending mode (kg)

η_i = bending displacement of the ith bending mode (m)

$Y_{\beta i}$ = bending mode shape at gimbal (unitless)

$Y_{\beta i}'$ = bending mode slope at gimbal (unitless)

Y_{sij} = deflection of the ith bending mode at the jth slosh mass location (unitless)

$C_{Z\eta i}$ = wind bending force coefficient for the ith bending mode (N/rad)

n_b = number of bending modes

n_s = number of slosh modes (determined by number of propellant tanks)

1 Introduction

The objective of this thesis is to explore methods of modeling the uncertainty and analyzing the robust stability of linear time-varying systems such as spacecraft attitude control systems. Polytopic and parameter dependent methods for modeling time-varying system uncertainty are reviewed. The performance and convenience of multiple linear matrix inequality methods of stability analysis are also analyzed. Further, these methods are expanded to predict the robust stability of linear time varying systems using gain margins and phase margin approximations. The described modeling and stability analysis methods are applied to a case study involving a launch vehicle attitude control system with rigid rotation, rigid translation, and sloshing fuel included in the dynamics.

Spacecraft attitude control systems in the aerospace industry can be modeled as linear time-varying systems. Most control systems must be stable throughout the entire time of flight. This is certainly the case in a crew launch vehicle, where instability can lead to mission failure and the loss of several lives and millions of dollars [1]. One approach to analyzing the stability of spacecraft attitude controls systems is using the frozen-time analysis technique, which assumes that control system parameters hold constant over a short period of flight time. Frequency domain methods, including Nyquist, Nichols, and Bode plots, μ-analysis, characteristic gain frequency, and Hurwitz stability criteria are then used to analyze system stability and robustness, even though they are intended for time-invariant systems [1][2][3][4][5]. Since a real spacecraft attitude control system is time-varying, the stability prediction from a frozen time analysis must be verified via a time varying technique. Further, Monte Carlo analysis has been used to check the robustness of spacecraft attitude control system. The Monte Carlo

screening technique, which is widely accepted as a valid analysis, can be quite time-consuming and computationally costly due to the large number of realizations required to account for all possible operating conditions [1][6][7][8]. Moreover, it is still frequently associated with frozen time analysis. In this thesis, an alternative stability analysis approach is taken; a time-varying stability analysis approach is developed to predict the robust stability of a linear control system without the frozen time assumption.

Time-varying stability analysis techniques have been applied to industry control systems for decades. One technique, commonly known as quadratic stability, is based on Lyapunov stability theory and assumes the time varying system can change infinitely fast. This method can effectively predict stability of a time-varying system; the results, however, tend to be conservative, meaning that a system that is actually stable for the tested operating conditions may be deemed unstable because of the infinite rate assumption [9][10][11]. In the real application, the control system parameters often vary slowly or at finite rates. With the rate information, Lyapunov stability criteria can be used to better estimate the robustness of the time varying spacecraft attitude control system. While available literature shows that parameter dependent Lyapunov functions provide a less conservative method for evaluating the stability and performance of time-varying systems, the application of these methods to large complicated spacecraft-type systems is not as well documented [11][12][13].

There is a need for a less conservative method of stability analysis to evaluate the stability and robustness of a time-varying control system. Further, the method must take into consideration the rate of change of the system and/or its parameters to minimize conservatism while still ensuring that the system is stable over the relevant time intervals.

The method must be applicable to several different systems and should be able to handle multiple combinations of uncertain and/or time-varying parameters. Finally, the method must be suitable for the evaluation of the robustness of a linear time-varying system in the form of gain and phase margins.

This thesis seeks to review and analyze techniques that can be applied to time-varying linear systems to assess their robust stability. For this reason it is advantageous to limit the number of simplifications and assumptions. On the other hand, it is necessary to implement a number of simplifications and assumptions that limit its scope in the interests of making efficient use of available tools.

Many mechanical systems, including the launch vehicle considered in the case study, depend on many uncertain time-varying parameters. However, for many of the methods considered in this thesis, treating all of those parameters as uncertain and/or time varying would lead to excessive computation times and, perhaps, conservative results. Therefore, the thesis treats only a small number of parameters as uncertain and time-varying at a time while holding the other parameters at their nominal, time-invariant values. To account for this simplification, several parameters and combinations are considered for each system.

The case study used to showcase the methods discussed in the thesis features a numerical example of the robustness and stability analysis for a crew launch vehicle. Not only does this kind of system involve several time-varying parameters, but it also involves a complicated mathematical model representing the spacecraft dynamics [14]. To evaluate this case study efficiently, the following simplifications are made.

The aforementioned launch vehicle example has the potential to feature rotational and translational dynamics for roll, pitch, and yaw. Roll, however, is omitted because it is modeled in a non-linear fashion [15]. Since pitch and yaw are assumed to be essentially symmetrical and negligibly coupled, only yaw dynamics is considered in this case study to reduce the size of the system model [1].

The full dynamics of the numerical launch vehicle example dictates that if bending motion is included, a flex filter is required to guarantee stability even for the nominal operating condition [1][2]. Since including this filter increases the size and complexity of the linear system, it also increases the required computation time for stability analysis. Therefore, the case study initially considers the numerical example without the bending dynamics and the flex filter. These parts of the system are then reinstated to in an attempt to apply the methods at hand still apply to the more complicated system even though it is more computationally demanding.

The bending and slosh dynamics of the launch vehicle in the case study example are simplified in the example to only include the two largest modes. For the bending dynamics, these are the two bending modes with the largest nominal magnitude of response because they are preserved by the filter [1][16]. In the slosh dynamics, the slosh characteristics for the two largest fuel tanks on the vehicle are considered.

The chapters in this thesis are organized as follows:

Chapter 2 provides an overview of uncertain linear systems and outlines various methods of modeling different kinds of uncertainty in them. This includes a discussion

on which modeling methods are most suitable for capturing the dynamics of systems subject to time-varying parameters and uncertainties.

Chapter 3 presents multiple methods for analyzing the stability of linear systems, based on the models featured in Chapter 2. After a discussion of the theory, a spring-mass-damper system is used as an example of a simple mechanical linear system to portray the relative strengths and weaknesses of several of the stability tests deemed most applicable to time-varying systems.

Chapter 4 discusses methods for extending the tools and theories in Chapter 3 to include stability margins as a measure of system robustness.

Chapter 5 applies the methods featured in the previous three chapters to analyze a numerical case study evaluating the robust stability of a crew launch vehicle. The chapter commences with an overview of the relevant spacecraft dynamics and necessary assumptions. Initially, the bending dynamics and the flex filter are ignored to reduce the complexity of the system and to allow for more in-depth analysis without excessive computation time. The stability criteria described in Chapter 3 are applied to create stability envelopes for multiple time-varying parameters. The methods illustrated in Chapter 4 are utilized to perform a robustness analysis on the spacecraft model. Subsequently, bending dynamics and a flex filter are reintroduced into the system to create a higher fidelity spacecraft model for future analysis with similar methods.

Finally, Chapter 6 summarizes the findings and draws conclusions from the results of previous chapters and suggests themes and directions for future research.

2 Linear Time-Varying Systems

This chapter provides an overview of time-varying linear systems. First, the basic concepts of linear control systems are reviewed. Subsequently, it details different methods of modeling linear systems and uncertainty therein. The advantages and limitations of these methods concerning their applicability to time-varying systems are also discussed throughout.

2.1 Review of Linear Systems

The brief overview of linear systems presented in this section is primarily based on information available in [17], [18], and [19].

A "control system" is "an arrangement of physical components connected or related in such an manner as to command, direct, or regulate itself or another system" [17]. A control system is often defined by the relationship between its input, the stimulus or command applied to the system, and its output, the response to that stimulus. The properties of a physical system dictate the form in which the input-output relationship is expressed. Considering a system for which the input $u_1(t)$ creates the output $y_1(t)$ and the input $u_2(t)$ produces the output $y_2(t)$ that is initially at rest (i.e. initial conditions are all zero). The system is linear if the input $c_1 u_1(t) + c_2 u_2(t)$ yields the output $c_1 y_1(t) + c_2 y_2(t)$ for all constants c_1 and c_2 and inputs $u_1(t)$ and $u_2(t)$ [17].

Alternatively, a system is linear if the input-output relationship can be described by the equation,

$$y(t) = \int_{-\infty}^{\infty} h(t, \tau) u(\tau) d\tau, \tag{2.1}$$

with the assumption again that the system is initially at rest, and $y(t)$ is the output, or forced response, $u(t)$ is the input, and $h(t, \tau)$ is a function that embodies the internal properties of the system and quantifies the response to the impulse $\delta(t - \tau)$ applied at time τ [17][19].

The outputs of many physical systems depend only on past and/or present values of the inputs. This concept, known as causality, also places a restriction on the form of the output. If a linear system is causal, Equation 2.1 becomes

$$y(t) = \int_{-\infty}^{t} h(t, \tau) u(\tau) d\tau, \tag{2.2}$$

which is equivalent to setting $h(t, \tau)$ equal to zero for $\tau > t$ in Equation 2.1. Moreover, a linear system is finite-dimensional if the input-output relationship is characterized by a linear differential equation of the form

$$y^{(n)}(t) + \sum_{i=0}^{n-1} a_i(t) y^{(i)}(t) = \sum_{i=0}^{m} b_i(t) u^{(i)}(t). \tag{2.3}$$

In this equation, $y^{(i)}(t)$ is the ith time derivative of $y(t)$, $u^{(i)}(t)$ is the ith time derivative of $u(t)$ $a_i(t)$ and $b_i(t)$ are real functions representing the system behavior, n is the order of the differential equation with respect to $y(t)$, and $m \leq n$ is the order with respect to $u(t)$.

As suggested by the time dependence in Equations 2.2 and 2.3, linear systems are, in general, time-varying. A system described by Equation 2.2 is time-invariant if and only if

$$h(t + \gamma, \tau + \gamma) = h(t, \tau), \quad \forall \, t, \tau, \gamma \in \mathbb{R}. \tag{2.4}$$

Likewise, a system in the form of Equation 2.3 is only time-invariant if $a_i(t) = a_i$ and $b_i(t) = b_i$, for all $i = 1, 2, \dots n - 1$.

In certain cases, it is useful to describe a system with a set of first order linear differential equations instead of one or more higher-order equations in the form of Equation 2.3. To accomplish this task, the state vector, output vector, and input vector are designed, and linear algebra concepts are used to develop coefficient matrices that represent system behavior. An n -dimensional linear system with m inputs and p outputs can be represented with the state model

$$E(t)\dot{x}(t) = A(t)x(t) + B(t)u(t) \qquad (2.5)$$

$$y(t) = C(t)x(t) + D(t)u(t). \qquad (2.6)$$

In this system, Equation 2.5 is the state equation, Equation 2.6 is the output equation, $A(t)$ is the system matrix, $B(t)$ is the input matrix, $C(t)$ is the output matrix, $D(t)$ is the direct feed matrix, $x(t)$ is the n –dimensional state vector, $y(t)$ is the p –dimensional output vector, and $u(t)$ is the m –dimensional input vector. Guidelines and simple examples on transforming linear systems into state model representations are available in [17] and [18].

In many physical systems, the time-varying nature of the matrices in the state model results from a dependence on one or more time-varying parameters. In this case, Equations 2.5 and 2.6 can be expressed as

$$\dot{x}(t) = A(p(t))x(t) + B(p(t))u(t) \qquad (2.7)$$

$$y(t) = C(p(t))x(t) + D(p(t))u(t), \qquad (2.8)$$

where $p(t)$ is a vector of the parameters upon which the linear system depends. This notion of parameter dependence is considered further in the following sections devoted to uncertainty and modeling.

2.2 Modeling Uncertain Linear Time-Varying Systems

As suggested by the previous section, real world systems are analyzed by modeling them with one or more equations. However, equations, especially linear equations, cannot always capture the true dynamics of the real world system or predict disturbances that may affect it. While not all uncertainty can be predicted and/or modeled, a mathematical model that accounts for more uncertainty will yield a control system that is more likely to be stable and meet performance requirements in all operating conditions. There are many options for modeling uncertainty in a control system, and each lends itself to different methods of analysis.

2.2.1 Linear Fractional Transformation

Linear fractional transformation (LFT) is a method in which uncertainty is modeled as a separate system from the known, or nominal, portion of the model. It can be used to model several different kinds of uncertainty, and it is suitable for stability analysis by way of several different methods, including μ-analysis, characteristic gain frequency, and non-linear methods like Popov criterion [1][9][20].

It is common for LFT models to be portrayed with block diagrams. Figure 2.1 shows two representations of a general LFT uncertain system model. Notice that LFT models can be utilized in either the frequency domain (Figure 2.1(a)) or the time domain (Figure 2.1(b)).
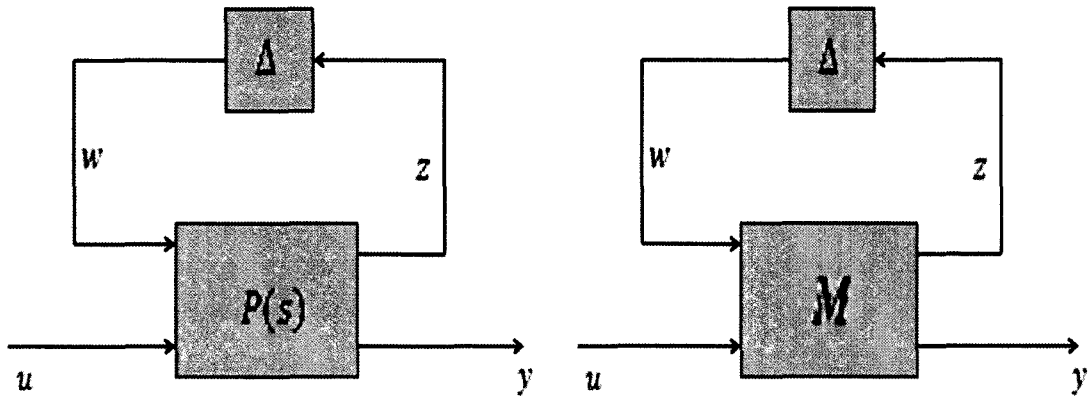
Figure 2.1: (a) Frequency Domain and (b) Time Domain LFT Representation

In the figures above, the uncertain system has input, u, and output, y. $P(s)$ and M represent a time-invariant transfer function and a block matrix, respectively. The symbol Δ denotes the system uncertainty, structured as a transfer function or matrix relating a fictitious output, z, to a fictitious input, w [21].

To understand how to model uncertainty using linear fractional transformation, consider an uncertain coefficient or parameter, p, with input, u, and output, y, portrayed in equation and block diagram form in Equation 2.9 and Figure 2.2, respectively.

$$y = pu = \left(p_0 + \delta_p\right)u \tag{2.9}$$
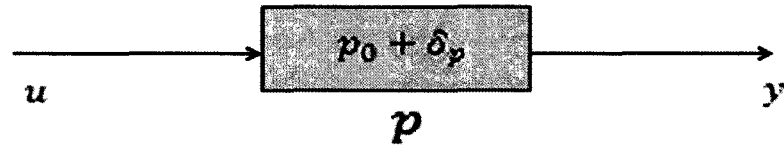
Figure 2.2: Block Diagram Representation of Uncertain Parameter

Above, p_0 represents the nominal value of the parameter and δ_p represents any variation

from the nominal [1]. An equivalent LFT uncertain system model for p is shown in

Figure 2.3.
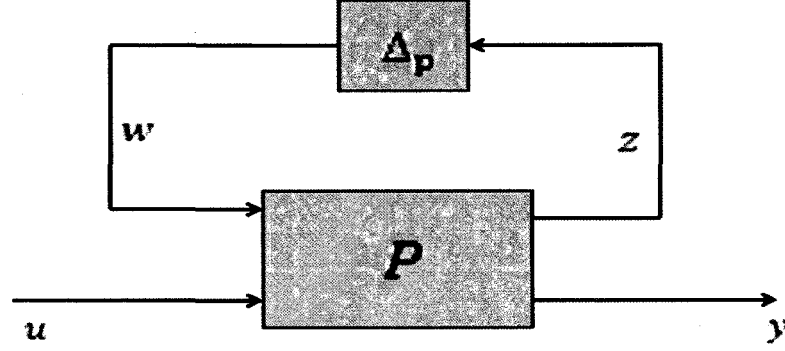
In the LFT above, P is a block matrix representing the nominal system in the form

of

$$P = \begin{bmatrix} P_{11} & P_{12} \\ P_{21} & P_{22} \end{bmatrix} \tag{2.10}$$

and Δ_p represents the uncertainty and can take the form of a scalar or a matrix depending

on the parameter's structure [1]. Combining the equations for z, y, and w,

$$z = P_{11}w + P_{12}u, \tag{2.11}$$

$$y = P_{21}w + P_{22}u, \tag{2.12}$$

and

$$w = \Delta_p z, \tag{2.13}$$

yields an alternative expression for the relationship between u and y, [22]

$$y = (P_{22} + P_{21}\Delta_p(I - P_{11}\Delta_p)^{-1}P_{12})u. \tag{2.14}$$

The last step for completing the uncertain system for p is to choose values for the block

elements of P such that Equations 2.9 and 2.14 are equivalent. One example of a method

for selecting these elements along with an example LFT model for a spacecraft can be

found in [1].

A system model formed using linear fractional transformation can be a powerful

tool for analyzing stability and robustness for many different examples of uncertain

control systems. However, time-varying systems pose certain shortcomings of LFT.

Since the nominal blocks must be time-invariant, time-varying elements of the system are

generally modeled as part of the uncertainty [9]. While one of the strengths of LFT is

that it can be used for an array of different analysis and design methods, some of the

methods, such as μ-analysis and characteristic gain frequency, assume time-invariance

[1]. Time-varying LFT models, therefore, are typically analyzed with non-linear methods

such as Popov's criterion [9]. These methods, used to predict absolute stability, may

yield conservative results, especially for linear systems. Moreover, LFT models

generally do not take into consideration the finite rates for slowly time-varying systems.

2.2.2   Uncertain State Space Models

As mentioned in the overview of linear systems, state-space form is a convenient

and powerful way of modeling and analyzing control systems. Linear systems with

uncertainty that meets certain requirements, to be explained later in this section, can be

described with the uncertain state space model,

$$E(t)x(t) = A(t)x(t) + B(t)u(t) \tag{2.15}$$

$$y(t) = C(t)x(t) + D(t)u(t), \tag{2.16}$$

where $A(t)$, $B(t)$, $C(t)$, $D(t)$, and $E(t)$ are all uncertain and/or time-varying matrices. The remainder of this section will discuss how this structure can be used to model different types of uncertainty.

2.2.2.1 Polytopic Systems

The equations and concepts presented in this section can be traced in the developments of [9].

A polytopic system is a linear time-varying system of the form of Equations 2.15 and 2.16 with uncertainty such that the matrix,

$$S(t) = \begin{bmatrix} A(t) + jE(t) & B(t) \\ C(t) & D(t) \end{bmatrix}, \tag{2.17}$$

varies inside a given convex polytope of matrices,

$$S(t) \in Co\{S_1, \dots, S_k\} := \sum_{i=1}^{k} \alpha_i S_i : \quad \alpha_i \geq 0, \ \sum_{i=1}^{k} \alpha_i = 1. \tag{2.18}$$

In this polytope, $S_1, \dots, S_k$ are constant vertex systems such that

$$S_i = \begin{bmatrix} A_i + jE_i & B_i \\ C_i & D_i \end{bmatrix}. \tag{2.19}$$

For a detailed description of the concept of convex polytopes, refer to [23]. Polytopic models can be useful in several cases, including modeling a system that changes between different sets of operating conditions, some non-linear systems, or systems that are

affinely dependent on uncertain or time-varying parameters. The following section discusses systems of the latter category.

2.2.2.2 Affine Parameter Dependent Systems

The equations and concepts presented in this section can be traced in the developments of [9].

Linear control systems that vary as a result of their dependence on uncertain or time-varying parameters can be represented using the uncertain state-space model of a parameter dependent system (PDS),

$$E(p(t))\dot{x}(t) = A(p(t))x(t) + B(p(t))u(t) \qquad (2.20)$$

$$y(t) = C(p(t))x(t) + D(p(t))u(t), \qquad (2.21)$$

where p represents a vector of uncertain or time-varying parameters. Systems with dependence on p such that

$$S(p) = \begin{bmatrix} A(p) + jE(p)) & B(p) \\ C(p) & D(p) \end{bmatrix}, \qquad (2.22)$$

$$A(p) = A_0 + p_1 A_1 + p_2 A_2 + \cdots + p_n A_n, \qquad (2.23)$$

$$B(p) = B_0 + p_1 B_1 + p_2 B_2 + \cdots + p_n B_n, \qquad (2.24)$$

$$\vdots$$

$$S(p) = S_0 + p_1 S_1 + p_2 S_2 + \cdots + p_n S_n \qquad (2.25)$$

are referred to in the literature as affine PDSs and are well suited for several different analysis methods. Refer to [23] for more information on affine sets and relationships. In these system models, each element of **p** represents a parameter and is defined with a range of extreme values,

$$p_i \in [\underline{p_i}, \overline{p_i}], \tag{2.26}$$

and upper and lower bounds on its rate of change,

$$\underline{\dot{p}_i} \le \dot{p}_i(t) \le \overline{\dot{p}}_i. \tag{2.27}$$

Also known as the "bounding box" method, this process creates a multi-dimensional box within which all parameter variations occur [24]. As stated in the previous chapter, the inclusion of bounds on the rate of variation in time-varying stability analysis can effectively reduce the conservatism of the results. This characteristic makes PDS modeling a powerful tool for evaluating the types of systems considered in this thesis.

Another possibly useful characteristic of an affine PDS model is that it can be transformed into a polytopic model by calculating the system's matrices at each vertex, Π_i, where $i = 1,2, \ldots 2^n$ and n is the number of uncertain parameters. Figure 2.4 presents a simple illustration of how a set of parameter vertices can be mapped to a polytope of systems.
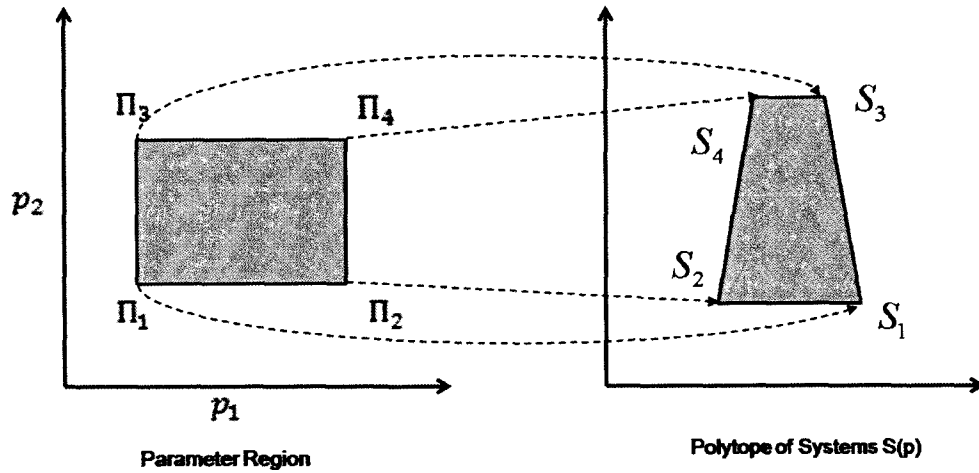
Figure 2.3: Mapping an Affine PDS Model to a Polytopic System Model

In performing this transformation, however, the rate information on each individual

parameter is typically lost in the polytopic analysis. Since the lack of a finite rate bound

leads to the assumption that the system parameters can vary arbitrarily fast, this sort of

transformation is most effective for rapidly time-varying systems.

2.2.2.3 Higher-Order Parameter Dependent Systems

The concepts and equations presented in this section can be traced in [11].

While many linear control systems can be seamlessly modeled by affine PDSs,

others have a higher-order dependence on uncertain time-varying parameters. In other

words, the parameters appear in the system in such a manner that they are multiplied by

one another in one or more instances. Modeling these systems affinely would require

treating higher-order terms as separate parameters. This, in turn, would require real

interval arithmetic [25] to determine the correct bounds on the range and rate of the new

parameters in addition to adding to the overall number of parameters.

Instead of creating separate higher-order parameters, [11] introduces a method by which higher-order parameter dependent systems can be modeled. In this context, consider the homogeneous, or zero input, time-varying linear system,

$$\dot{x}(t) = A(\delta(t))x(t), \tag{2.28}$$

where $\delta(t)$ is a vector of time varying parameters [26]. To express the system in terms of its parameter dependence, let

$$\dot{x} = A(\delta)x = \sum_{i=0}^{q} A_i \pi_i, \tag{2.29}$$

where $i = 0, \dots, q - 1$ and

$$\pi_{i+1} = \Theta_i(\delta)\pi_i, \qquad \pi_0 = x. \tag{2.30}$$

In this formulation, $\Theta_i(\delta)$ are affine matrices containing elements of $\delta(t)$, π_i are auxiliary functions of x and $\delta(t)$ used to capture the dependence on higher-order parameters, A_i are constant matrices representing the known elements of the system, and q represents the highest order of parameter dependence.

Figure 2.4 shows a block diagram of the system model presented in Equations 2.29 and 2.30 that helps to visualize how the parameters in each Θ_i are multiplied together to represent higher-order parameter dependence.

Once the matrices in the system are defined, it is possible to show the separation the known elements of the system and the unknown parameters. These steps are shown in Figure 2.5 and Equations 2.31 and 2.32.
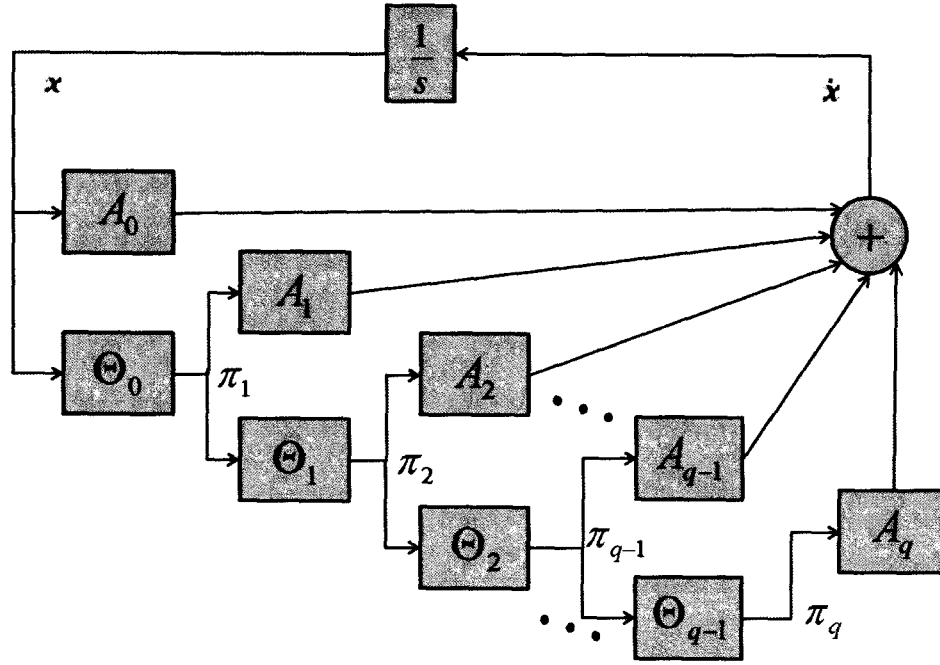
Figure 2.4: Block Diagram of Higher-Order PDS Model
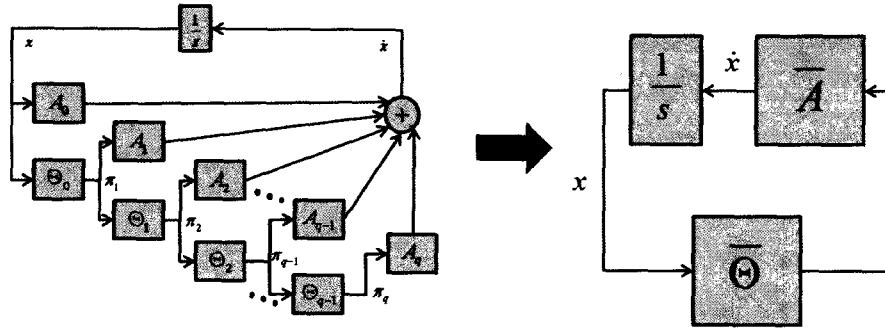
Figure 2.5: Simplified Block Diagram of Higher-Order PDS Model

$$\bar{A} = [A_0 \quad A_1 \quad ... \quad A_q] \tag{2.31}$$

$$\bar{\Theta} = \begin{bmatrix} I_{nx} \\ \Theta_0 \\ \Theta_1 \Theta_0 \\ \vdots \\ \Theta_{\tilde{q}-1} \cdots \Theta_1 \Theta_0 \end{bmatrix} \tag{2.32}$$

Note that the selection of the Θ_i matrices is not unique. More guidelines for choosing the structure of these matrices to aid in stability analysis are presented in the next chapter.

3 Stability Analysis for Linear Time-Varying Systems

3.1 Stability

The response, or output, of a control system is comprises the natural response and the forced response. The natural response describes whether a system dissipates, maintains, or acquires energy. It is a function only of the system dynamics and is independent of the system's input. The forced response, on the other hand, is a function of the input to the system. For linear systems, these two parts are summed to create the total response of the system [18].

As stated in Chapter 2, the objective of a control system is to command, direct, or regulate [17]. For this to be possible, the natural response must either dissipate or maintain energy so that the system's input can control the response. Systems that acquire energy may have a natural response that increases in magnitude in an unbounded fashion, eventually rendering the control input useless and leaving the control system unable to regulate or direct the response. The latter condition is known as instability [18].

Stability, therefore, is a term used to describe the natural, or homogenous, response of a system. A system is stable if its natural response decays to zero as time approaches infinity. A marginally stable system is one whose natural response does not approach zero but oscillates within a bounded region. In marginally stable systems, however, bounded inputs may cause an unbounded response. Therefore, marginally stable systems will henceforth be considered unstable in this thesis [17][18].

3.2 Time-Invariant Stability Analysis Review

As mentioned above, a control system's natural response is determined by the system dynamics which, as suggested in Chapter 2, is often modeled with one or several linear differential equations. Therefore, stability analysis involves obtaining information about the natural response from a system's mathematical model. There are several commonly used methods for determining the natural response characteristics, and thus the stability, of linear time-invariant (LTI) systems.

One such method of determining stability involves expressing the mathematical model in the frequency domain. For instance, performing a Laplace transform [17],

$$\mathcal{L}[f(t)] = F(s) = \int_{0_-}^{\infty} f(t)e^{-st}dt, \tag{3.1}$$

on the system equation and setting initial conditions to zero creates a transfer function of the form,

$$Y(s) = G(s)U(s), \tag{3.2}$$

where s represents the complex number $s = \sigma + j\omega$, $Y(s)$ is the Laplace transform of the system response, $U(s)$ is the Laplace transform of the input, and $G(s)$ is the transfer function which relates the output to the input. For more information and examples on using Laplace transforms to create transfer functions, consult [18].

Using Equation 3.1 or a table of Laplace transforms, it can be confirmed that the transforms,

$$f(t) = e^{-at}u(t) \Leftrightarrow F(s) = \frac{1}{s+a}, \tag{3.3}$$

are true, where $u(t)$ is a unit-step input such that

$$u(t) = \begin{cases} 0, & t < 0 \\ 1, & t > 0 \end{cases} \tag{3.4}$$

and a is a complex number. In Equation 3.3, the value $s = -a$ is known as a pole, or a value of s which causes the transfer function to become infinite. From the transformation it follows that a pole with a negative real value creates an exponential decay in the response, where as a pole with a positive real value yields a response with exponential growth. Since exponential growth is unbounded, a positively real valued pole yields instability. Conversely, a negatively real valued pole goes to zero as time goes to infinity, indicating a stable system.

For linear systems with multiple poles, the transfer function takes the general form

$$G(s) = \frac{N(s)}{D(s)} = \frac{N(s)}{(s+p_1)(s+p_2)...(s+p_m)...(s+p_n)}. \tag{3.5}$$

Using partial fraction expansion, this transfer function becomes

$$G(s) = \frac{K_1}{(s+p_1)} + \frac{K_2}{(s+p_2)} + \cdots \frac{K_m}{(s+p_m)} + \cdots \frac{K_n}{(s+p_n)}, \tag{3.6}$$

where $K_1 ... K_n$ are constants, known as residues, which take the place of the transfer function numerator. Notice that for any of the poles $s = -p_i$ for $i = 1 ... n$, the value of the entire transfer function goes to infinity in both Equations 3.5 and 3.6. Also, the Linearity Theorem for Laplace transforms,

$$\mathcal{L}[f_1(t) + f_2(t)] = F_1(s) + F_2(s) \tag{3.7}$$

implies that the total response of the linear system can be obtained by summing the response created by each individual pole of the system's transfer function [18]. Therefore, if one transfer function pole causes a response that grows unboundedly, the total response is also unbounded. From all of this, the conclusion is drawn that for a LTI system to be stable, all the poles of its transfer function must have negative real parts [27].

This criterion for stability enables the use of several frequency domain methods for analyzing LTI systems including Routh-Hurwitz tables, Nyquist criterion, Nichols criterion, Bode plots, and root locus design. For more details on these frequency domain methods and relevant numerical examples, see [17] and [18].

Even though the preceding process involves analyzing the system in the frequency domain, system stability can also be related to the characteristics of the state space system, particularly the eigenvalues of the system matrix. Consider the state space system,

$$\dot{x}(t) = Ax(t) + Bu(t) \tag{3.8}$$

$$y(t) = Cx(t) + Du(t), \tag{3.9}$$

developed from the differential equations for a LTI system. Using the Laplace transform, these equations become

$$(sI - A)X(s) = x(0) + BU(s) \tag{3.10}$$

$$Y(s) = CX(s) + DU(s), \tag{3.11}$$

where I is an identity matrix with dimensions equal to those of A (i.e. an $n \times n$ matrix where n is the order of the linear system). Note that in Equations 3.10 and 3.11, the Laplace transform of a vector implies the transform of each of the elements. The transfer function is then formed by solving Equation 3.10 for $X(s)$, substituting into Equation 3.11, and evaluating the expression with zero initial conditions. That is,

$$G(s) = C(sI - A)^{-1}B + D, \tag{3.12}$$

where $G(s)$ represents the transfer function as shown in Equation 3.2. By the relationship between the inverse of a square matrix, M, to the determinant, $det(M)$, and the adjoint matrix, $adj(M)$,

$$M^{-1} = \frac{adj(M)}{det(M)}, \tag{3.13}$$

it follows that for values of s such that $det(sI - A) = 0$, the transfer function $G(s)$ becomes infinity [28]. Therefore, the roots of $det(sI - A) = 0$ are the poles of the system transfer function. For a square matrix, M, the roots of $det(sI - M) = 0$ are known as its eigenvalues [28]. It follows that for the linear system described in Equations 3.11 and 3.12 to be stable, its system matrix, A, must have eigenvalues with negative real values. These eigenvalues can be determined without resorting to the frequency domain to determine a system transfer function [18].

3.3 Time-Varying Stability Analysis

In industry, the criteria and methods outlined in the previous section are often used to analyze control systems by taking advantage of frozen time analysis. This

process involves using system information at a select set of times and analyzing the system under the assumption that the dynamics varies sufficiently slowly [1][2][3][4].

The methods mentioned above, however, may not be adequate for the analysis of the system response for time-varying systems. For example, time-varying linear systems are presented in [27] and [29] where either the system matrix eigenvalues are negatively real valued for all time but the system response grows unboundedly, or the system matrix has at least one positively real valued eigenvalue but its response is stable. Given these cases, a different set of criteria must be used to determine the stability of time-varying linear systems. Lyapunov stability theory presents an alternative set of tools for analyzing these types of systems.

3.3.1 Lyapunov Stability Theory

The objective of this section is to describe Lyapunov stability theory, more properly called Lyapunov's direct method, in a concise and comprehensible manner. Sources for more information on the basis and background of Lyapunov stability theory include [27], [30], or [31].

Consider a time-varying linear system with no external inputs, much like the homogeneous linear system in Equation 2.28, and that the system is at equilibrium when all of its states are zero valued. If a function $v(x, t)$ can be found, where x represents the system's state vector, t is time, and a, b, and c are positive constants such that the following are all true:

1) $v(0, t) = 0 \quad and \quad \dot{v}(0, t) = 0, \quad \forall t \in \mathbb{R}^+,$ (3.14)

2) $a\|x\|^2 \leq v(x, t) \leq b\|x\|^2, \quad \forall t \in \mathbb{R}^+ \ and \ \forall x \in \mathbb{R}^n ,$ (3.15)

and

$$3) \quad v(x,t) \leq c\|x\|^2, \quad \forall t \in \mathbb{R}^+ \text{ and } \forall x \in \mathbb{R}^n, \tag{3.16}$$

then the system is exponentially, or uniformly asymptotically stable [27]. That is, the response is bounded and approaches zero as time approaches infinity.

Obviously, the Lyapunov Direct Method seeks a function that represents, i.e. possesses the same properties as, the system's total energy. Like the total energy of a stable system, the value of this function is zero and at a local minimum when the states are zero, positive when the states are non-zero, and always decreasing from its initial value [30].

For the unforced linear time-varying system,

$$\dot{x}(t) = A(t)x(t), \tag{3.17}$$

the most common candidate Lyapunov function for linear systems takes the form

$$v(x,t) = x^T(t)P(t)x(t), \tag{3.18}$$

where $P(t)$ is an $n \times n$ matrix and n is the order of the system. Clearly, the quadratic dependency of this candidate function on the states dictates that it meets the first of the three criteria mentioned above in that its value is zero and at a local minimum when the states are equal to zero. For the function to be positively valued for non-zero state values, $P(t)$ must be positive definite (the definitions and explanations of "positive definite" and "negative definite" can be found in [32]), written

$$P(t) > 0. \tag{3.19}$$

Next, conditions are developed to show that the function is always decreasing. First, the

expression for the time derivative of the candidate function, Equation 3.18, is expanded

using the chain rule and the product rule [33]. Specifically,

$$\dot{v}(x, \dot{x}, t) = \frac{d(x^T(t)P(t)x(t))}{dt} < 0, \tag{3.20}$$

and

$$\frac{d(x^T(t)P(t)x(t))}{dt} = x^T(t)\frac{d(P(t)x(t))}{dt} + \frac{d\left(x^T(t)\right)}{dt}P(t)x(t)$$

$$= x^T(t)\frac{d(P(t)x(t))}{dt} + \frac{d\left(x^T(t)\right)}{dt}P(t)x(t) < 0$$

$$= x^T(t)\left[P(t)\frac{d(x(t))}{dt} + \frac{d(P(t))}{dt}x(t)\right] + \frac{d\left(x^T(t)\right)}{dt}P(t)x(t) < 0. \tag{3.21}$$

Next, Equation 3.17 is substituted into Equation 3.21, yielding

$$\dot{v}(x, \dot{x}, t) = x^T(t)\left[P(t)A(t)x(t) + \frac{d(P(t))}{dt}x(t)\right] + x^T(t)A^T(t)P(t)x(t) < 0. \tag{3.22}$$

Finally, factoring out the quadratic state vectors gives

$$\dot{v}(x, \dot{x}, t) = x^T(t)\left[P(t)A(t) + \frac{d(P(t))}{dt} + A^T(t)P(t)\right]x(t) < 0 \tag{3.23}$$

$$P(t)A(t) + \frac{d(P(t))}{dt} + A^T(t)P(t) < 0, \tag{3.24}$$

where Equation 3.24 states that the value on the left side of the inequality must be

negative definite.

Quadratic stability, named because of the candidate function's quadratic dependence on the state, is an extension of Lyapunov's Direct Method commonly associated with time-varying linear systems. For quadratic stability, the candidate function takes the form,

$$v(x, t) = x^T(t)Px(t). \tag{3.25}$$

Notice that the matrix, P, is now assumed to be constant. This assumption simplifies the conditions in Equations 3.19 and 3.24. Specifically,

$$P(t) > 0 \quad \Rightarrow \quad P > 0 \tag{3.26}$$

and

$$P(t)A(t) + \frac{d(P(t))}{dt} + A^T(t)P(t) < 0 \quad \Rightarrow \quad PA(t) + A^T(t)P < 0. \tag{3.27}$$

Since P is now a constant, its time derivative becomes zero, yielding Equations 3.26 and 3.27. If a constant matrix, P, meets the conditions in Equations 3.26 and 3.27 for all times $t_0 \leq t \leq \infty$, the time-varying system (Equation 3.17) is stable. Moreover, since Equation 3.27 no longer has a time derivative term, the system is stable even for a system $A(t)$ that varies arbitrarily fast, or $-\infty \leq \dot{A}(t) \leq \infty$.

Since quadratic stability evaluates the stability assuming that a system can vary arbitrarily fast, the resulting analysis is potentially conservative, especially for systems that vary slowly, or with rates of variation that are bounded by finite numbers. For example, the proof, summarized below and found in its entirety in [27], shows that LTI

stability criteria can accurately predict stability for time-varying systems with sufficiently slow rates of variation.

Consider again an unforced, time-varying system (Equation 3.17) and assume that

1) system matrix $A(t)$ is bounded such that

$$\|A(t)\| \leq m \ , \quad \forall t \in \mathbb{R}^+, \tag{3.28}$$

2) the eigenvalues of $A(t)$ are negatively real valued (recall that this would be enough to show stability if the system was time-invariant), and

3) there exists a positive scalar, ϵ, such that

$$\|\dot{A}(t)\| \leq \epsilon \ , \quad \forall t \in \mathbb{R}^+. \tag{3.29}$$

Due to the assumption that $A(t)$ has negatively real-valued eigenvalues (assumption 2 above), the Lyapunov equation,

$$P(t)A(t) + A^T(t)P(t) = -Q, \tag{3.30}$$

where Q is any constant positive definite matrix, yields a positive definite solution $P(t)$. It is important to realize that Equation 3.30 does not directly imply system stability because $P(t)$ is a function of time, but the $\frac{d(P(t))}{dt}$ term is absent, differentiating it from the stability criterion in Equation 3.24. This solution, $P(t)$ can be bounded as

$$\frac{\lambda_{min}(Q)}{2m} I \leq P(t) \leq \frac{k^2 \lambda_{max}(Q)}{2\alpha} I, \tag{3.31}$$

where $\lambda_{min}(Q)$ and $\lambda_{max}(Q)$ represent the minimum and maximum eigenvalues of Q, I represents the identity matrix with the same dimensions as $P(t)$, m is the positive scalar bound on the system matrix from Equation 3.28, and k and α are positive scalars

from the definition of exponential stability for a LTI system (the development of

Equation 3.30 and the use of k and α is described in detail in [27]). Next, the time

derivative of $P(t)$, written here as $\dot{P}(t)$, is added to both sides of Equation 3.30, and the

expression is given as

$$\dot{P}(t) + A^T(t)P(t) + P(t)A(t) = \dot{P}(t) - Q \leq \left(\left\| \dot{P}(t) \right\| - \lambda_{min}(Q) \right) I. \qquad (3.32)$$

Taking the time derivative of Equation 3.30 yields

$$A^T(t)\dot{P}(t) + \dot{P}(t)A(t) = -(\dot{A}^T(t)P(t) + P(t)\dot{A}(t)). \qquad (3.33)$$

Next, $\left\| \dot{P}(t) \right\|$ is given an upper bound using the same concepts that were used in

Equation 3.31 to bound $P(t)$ (except that $\dot{P}(t)$ cannot be assumed positive definite).

Specifically,

$$\left\| \dot{P}(t) \right\| \leq \frac{k^2 \left\| \dot{A}^T(t)P(t) + P(t)\dot{A}(t) \right\|}{2\alpha} \leq \cdots$$

$$\frac{k^2 \lambda_{max}(P(t)) \left\| \dot{A}(t) \right\|}{\alpha} \leq \frac{k^2 \lambda_{max}(Q)\epsilon}{2\alpha^2}. \qquad (3.34)$$

Finally, substituting this upper bound into Equation 3.32 yields

$$\dot{P}(t) + A^T(t)P(t) + P(t)A(t) \leq \left(\frac{k^2 \lambda_{max}(Q)\epsilon}{2\alpha^2} - \lambda_{min}(Q) \right) I. \qquad (3.35)$$

Clearly, for values of ϵ such that

$$\frac{k^2 \lambda_{max}(Q)\epsilon}{2\alpha^2} < \lambda_{min}(Q), \qquad (3.36)$$

the left side must be negative definite, meaning that the system is stable by Lyapunov's Direct Method. Due to the abstract values of k and α, this proof does not readily enable a simple quantitative analysis on whether or not time-invariant stability criteria are adequate for a given time-varying system. However, it suggests that as the bound on a system's rate of variation decreases, the range of operating conditions for which the system is stable will begin to resemble the corresponding range obtained with LTI stability criteria. Similar results for parameter dependent systems are presented in [34]. It is expected, therefore, that considering bounds on the system or its parameters' rates of variation will cause results from slowly varying systems to differ from quadratic stability results and resemble the results obtained from LTI stability analysis as the bounds decrease. The decreasing rate bounds may also lead to a decrease in the conservativeness of the results. These expectations are tested later in this chapter using a simple example of a time-varying linear system.

3.3.2 Linear Matrix Inequalities for Stability Analysis

The introductory paragraphs of this section present a brief introduction to linear matrix inequalities (LMIs) and their use in the analysis of control systems. They relate strongly to the material given in [22] and [35].

A linear matrix inequality takes the form,

$$F(x) \triangleq F_0 + \sum_{i=1}^{m} x_i F_i > 0 , \tag{3.37}$$

where F_i are given symmetric real matrices, x_i are real variables, and the "greater than" symbol states that the left side is positive definite. Equation 3.37 is referred to as a strict LMI, whereas the form,

$$F(x) \geq 0, \tag{3.38}$$

is a nonstrict LMI. This thesis, with the exception of the bounded rate proof in the previous section, deals with strict LMIs.

An LMI can be formulated to represent many different convex constraints on the variables x_i including linear and quadratic inequalities and matrix norm inequalities. Furthermore, multiple LMI's representing different constraints can be diagonally appended to each other to combine into a single, larger LMI. That is

$$F_1(x) > 0, \dots, F_p(x) > 0 \quad \Leftrightarrow \quad F(x) = \begin{bmatrix} F_1(x) & 0 & 0 \\ 0 & \ddots & 0 \\ 0 & 0 & F_p(x) \end{bmatrix} > 0. \tag{3.39}$$

The variables, x_i, in Equation 3.37 can also be matrices, as is the case in the Lyapunov stability criteria in Equations 3.19 and 3.24. For example, the Lyapunov inequality for quadratic stability,

$$PA + A^T P < 0, \tag{3.40}$$

can be transformed to resemble Equation 3.37. Let the symmetric matrix variable, $P = P^T$, comprise elements $P_1 \dots P_m$ such that

$$P = P^T = \begin{bmatrix} P_1 & P_2 & P_3 & \cdots & P_n \\ P_2 & P_{n+1} & P_{n+2} & \cdots & P_{2n-1} \\ P_3 & P_{n+2} & P_{2n} & \cdots & P_{3n-3} \\ \vdots & \vdots & \vdots & \ddots & \vdots \\ P_n & P_{2n-1} & P_{3n-3} & \cdots & P_m \end{bmatrix}, \tag{3.41}$$

where

$$m = n(n+1)/2 \tag{3.42}$$

and n is the order of the system (i.e. A and P are $n \times n$ matrices). Finally, let

$$F_0 = 0, \qquad F_i = -P_i A - A^T P_i \tag{3.43}$$

to complete the transformation.

The Lyapunov stability problem and others like it are known as feasibility problems. They are among the most common and basic LMI problems used in control systems analysis. As suggested by the name, the objective of such a problem is to either find a feasible solution, x, such that Equation 3.37 holds true, or establish that no such solution exists and the LMI is infeasible.

The previous section gave an overview of Lyapunov stability and how Lyapunov's Direct Method provided the basis of stability analysis criteria for time-varying systems. In the current section, it has been shown that LMIs provide a medium for using these criteria to evaluate control systems. Consider again, however, that the relevant control systems are time-varying. Therefore, in order for the system to be stable, the LMI problems presented by Lyapunov's criteria (as written in Equations 3.19 and 3.24) must be simultaneously feasible for all possible values of the system matrix $A(t)$. Solving this problem would, of course, require an infinite number of LMI formulations, and is therefore not a viable option [9][11].

In special cases like the systems modeled in the previous chapter, however, the number of LMIs can be reduced to a finite number, and thus incorporated into one larger LMI problem, based on the characteristics of the systems' uncertainty, time-variance, and/or parameter dependence. The sections that follow describe how this objective is accomplished for the three different types of system models presented in Chapter 2.

3.3.2.1 LMI Stability Analysis for Polytopic Models

Recall that the a polytopic model for a homogeneous linear time-varying system,

$$E(t)\dot{x}(t) = A(t)x(t), \tag{3.44}$$

varies such that $A(t) + jE(t)$ is bounded by a fixed convex polytope of matrices,

$$A(t) = \sum_{i=1}^{k} \alpha_i(t)A_i \tag{3.45}$$

$$E(t) = \sum_{i=1}^{k} \alpha_i(t)E_i \tag{3.46}$$

$$\alpha_i \geq 0, \ \sum_{i=1}^{k} \alpha_i = 1, \tag{3.47}$$

where k denotes the number of vertices of the polytope and α_i are the polytopic

coordinates of the matrices [9].

For quadratic stability, the system must meet the Lyapunov criteria

$$v(x, t) = x^T(t)Px(t) > 0 \tag{3.48}$$

and

$$\dot{v}(x, \dot{x}, t) = \frac{d(x^T(t)Px(t))}{dt} < 0, \tag{3.49}$$

where P is a constant matrix. For the system in Equation 3.44, these criteria reduce to

$$Q > 0 \tag{3.50}$$

and

$$E(t)QA(t)^T + A(t)QE(t)^T < 0, \tag{3.51}$$

where $Q = P^{-1} > 0$ is introduced to simplify the LMI in the presence of the matrix $E(t)$, which is assumed to be invertible. The fact that the systems range within a convex polytope asserts that the system is stable if each of its vertex systems are stable, reducing the number of constraints on the LMI to a finite quantity. Therefore, the system in Equation 3.44 is quadratically stable if a matrix $Q = Q^T > 0$ and scalars $t_{ij} = t_{ji}$ can be found such that

$$E_j Q A_i^T + A_i Q E_j^T + E_i Q A_j^T + A_j Q E_i^T < 2t_{ij}I \tag{3.52}$$

and

$$\begin{bmatrix} t_{11} & \cdots & t_{1k} \\ \vdots & \ddots & \vdots \\ t_{k1} & \cdots & t_{kk} \end{bmatrix} < 0, \tag{3.53}$$

where $i, j \in 1, \ldots, n$ and n is the number of vertex systems.

Furthermore, in cases where either $E(t)$ or $A(t)$ are constant, Equation 3.52 becomes a sufficient condition for quadratic stability, where $t_{ij} = 0$ [9].

As stated in Chapter 2, polytopic modeling does not account for information about the rate of change of the system or its parameters. Therefore, quadratic stability is the primary stability analysis criteria applicable to time-varying linear systems that are modeled using this method [9].

3.3.2.2 LMI Stability Analysis for Affine PDS Models

The equations, specifically the LMIs, and concepts presented in this section can be found in their original form in [9].

From Chapter 2, recall that an affine parameter dependent model for the homogeneous response of a system takes the form,

$$E(p(t))\dot{x}(t) = A(p(t))x(t), \tag{3.54}$$

where $p = [p_1\ p_2\ ...\ p_n]^T$ is a vector of uncertain parameters, and

$$A(p) = A_0 + p_1 A_1 + p_2 A_2 + \cdots + p_n A_n \tag{3.55}$$

$$E(p) = E_0 + p_1 E_1 + p_2 E_2 + \cdots + p_n E_n. \tag{3.56}$$

Each parameter, p_i, and its rate of variation, $\dot{p}_i$, are bound as shown in Equations 2.26 and 2.27, creating a hyper-rectangular parameter box within which the parameter vector and its rates can vary. Assuming each parameter has a range and a rate interval, the resulting parameter region has $2n$ dimensions, and thus has 2^{2n} vertices [24][36]. Due to the affine dependence on the parameters and the convex nature of the parameter box, stability can be determined by analyzing the systems at the vertices of the box instead of at every possible operating condition. Therefore, let

$$\mathcal{V} = \{(\omega_1, \omega_2, ..., \omega_n): \omega_i \in \{\underline{p_i}, \overline{p_i}\}\} \tag{3.57}$$

represent the vertices of the hyper-rectangle of parameter ranges, and

$$\mathcal{T} = \{(\tau_1, \tau_2, ..., \tau_n): \tau_i \in \{\underline{\dot{p}_i}, \overline{\dot{p}_i}\}\} \tag{3.58}$$

represent the vertices of the hyper-rectangle of parameter rates of variation. The overall parameter box is thus defined by

$$(\omega, \tau) \in \mathcal{V} \times \mathcal{T}. \tag{3.59}$$

To take advantage of the information provided by the parameter box, parameter dependent models are often analyzed using parameter dependent Lyapunov functions. The form of an affine parameter dependent Lyapunov function is

$$v(x, p(t)) = x^T(t)P(p)x(t) = x^T(t)Q^{-1}(p)x(t) > 0, \tag{3.60}$$

where

$$Q(p) = Q_0 + p_1 Q_1 + p_2 Q_2 + \cdots + p_n Q_n. \tag{3.61}$$

For this Lyapunov function, the stability criteria of Equations 3.48 and 3.49 become

$$Q(p) > 0 \tag{3.62}$$

and

$$E(p)Q(p)A(p)^T + A(p)Q(p)E(p)^T - E(p)\frac{d(Q(p))}{dt}E(p)^T < 0, \tag{3.63}$$

where

$$\frac{d(Q(p))}{dt} = \frac{d(Q_0 + p_1 Q_1 + p_2 Q_2 + \cdots + p_n Q_n)}{dt}$$

$$= \dot{p}_1 Q_1 + \dot{p}_2 Q_2 + \cdots + \dot{p}_n Q_n$$

$$= Q(\dot{p}) - Q_0. \tag{3.64}$$

The system, Equation 3.54, is stable if matrices $Q_0 = Q_0^T$, $\{Q_i = Q_i^T\}_{i=1}^n$ and $\{M_i = MiTi=1n\geq 0$ can be found such that the criteria

$$E(\omega)Q(\omega)A(\omega)^T + A(\omega)Q(\omega)E(\omega)^T -$$

$$E(\omega)(Q(\tau) - Q_0)E(\omega)^T + \sum_i \omega_i^2 M_i < 0, \tag{3.65}$$

$$E_i Q(\omega) A_i^T + A_i Q(\omega) E_i^T + E(\omega) Q_i A_i^T + A_i Q_i E(\omega)^T +$$

$$E_i Q_i A(\omega)^T + A(\omega) Q_i E_i^T + M_i \geq 0, \tag{3.66}$$

and

$$Q(\omega) > 0 \tag{3.67}$$

are met at all of the vertices of the parameter region, $\mathcal{V} \times \mathcal{T}$. In the preceding criteria, Equation 3.66 is referred to as the multi-convexity constraint. For a more detailed discussion on the origin of this constraint (with slightly different notation), refer to [37]. For the purpose of this thesis, it suffices to know that this constraint places a geometric constraint on the system to enable stability analysis by testing only at the vertices of the parameter region [38]. Furthermore, it is only necessary for parameters that enter two or more of the matrices $E(p)$, $A(p)$, and/or $Q(p)$ [9].

Recall that for quadratic stability, all parameters are assumed to change arbitrarily fast. If this is the case, Equations 3.65, 3.66, and 3.67 can only be found feasible if $\{Q_i = 0\}_{i=1}^n$. Therefore, if matrices $Q = Q^T > 0$ and $\{M_i = M_i^T\}_{i=1}^n \geq 0$ can be found such that

$$E(\omega)QA(\omega)^T + A(\omega)QE(\omega)^T + \sum_i \omega_i^2 M_i < 0 \tag{3.68}$$

and

$$E_j Q A_i^T + A_j Q E_i^T + M_i \geq 0, \tag{3.69}$$

the system in Equation 3.52 is quadratically stable for the specified uncertain parameters.

Note that in the case of quadratic stability, the Lyapunov function is no longer dependent

on the uncertain parameters, or $\{Q_i = 0\}_{i=1}^n$. Therefore, if $E(p)$ and $A(p)$ do not share a

dependence on any of the parameters, p_i, (i.e. $\{E_i = 0 \;\; or \;\; A_i = 0\}_{i=1}^n$) then the

multiconvexity constraint, Equation 3.69, can be removed and it is sufficient to evaluate

Equation 3.51 at the vertices of the parameter region [9].

3.3.2.3 LMI Stability Analysis for Higher-order PDS Models

In industrial application, modeling some systems as affinely parameter dependent

would require making new parameters to represent instances where parameters were

multiplied together. Creating more parameters increases the number of vertices that must

be tested with the LMIs. Moreover, using interval math to get the range and rate

information of these new parameters can create more conservativeness unless each

parameter is individually inspected [25]. To circumvent these difficulties, it is useful to

have a set of stability criteria, in the form of LMIs, for higher-order parameter dependent

system models.

One example of such a set is presented in [11] and is presented in an abridged

form in the current section.

Consider the homogeneous parameter dependent system,

$$\dot{x}(t) = A\big(\delta(t)\big)x(t), \tag{3.70}$$

where $\delta(t)$ is a vector of time varying parameters, analogous to $p(t)$ in the previous

section. Recall that this system can be modeled as higher-order parameter dependent

using Equations 2.29, 2.30, and 2.31. Similar to the previous section, a parameter

dependent Lyapunov function,

$$v(x, \delta) = x(t)^T P(\delta(t)) x(t), \qquad (3.71)$$

is utilized, rendering the stability criteria

$$P(\delta) > 0; \ \forall(\delta, \dot{\delta}) \in \beta \qquad (3.72)$$

and

$$\dot{P}(\delta, \dot{\delta}) + A(\delta)'P(\delta) + P(\delta)A(\delta) < 0; \ \forall(\delta, \dot{\delta}) \in \beta. \qquad (3.73)$$

In these equations, β denotes the region of parameter ranges and rates being tested.

Further,

$$P(\delta) = P(\Theta(\delta)) = \begin{bmatrix} I \\ \Theta(\delta) \end{bmatrix}^T P \begin{bmatrix} I \\ \Theta(\delta) \end{bmatrix}, \qquad (3.74)$$

where

$$P = \begin{bmatrix} P_0 & P_1 \\ P_1{}^T & P_2 \end{bmatrix} \qquad (3.75)$$

and $\Theta(\delta)$ is an affine matrix function of the parameters in δ.

As with the systems in the previous two sections, LMI conditions must be

formulated such that the system can be proven stable while limiting the LMIs to a finite

number. This is accomplished by creating LMIs that are affine in δ and $\dot{\delta}$, even though

the system itself may be higher-order parameter dependent. Given the definitions

$$A_{a1} = \begin{bmatrix} A_0 & A_1 \\ \dot{\Theta}_0 + \Theta_0 A_0 & \Theta_0 A_1 \end{bmatrix}, \tag{3.76}$$

$$A_{a2} = \begin{bmatrix} A_2 & \cdots & A_q \\ \Theta_0 A_2 & \cdots & \Theta_0 A_q \end{bmatrix}, \tag{3.77}$$

$$C_{a_1} = [\Theta_0 \quad -I_{m_1}], \tag{3.78}$$

and

$$C_{a_2} = \begin{bmatrix} \Theta_0 & -I_{m_1} & 0 & 0 \\ 0 & \ddots & & 0 \\ 0 & 0 & \Theta_{\tilde{q}-1} & -I_{m_{\tilde{q}}} \end{bmatrix}, \tag{3.79}$$

a system of the form of Equation 3.70 is stable for values of $(\dot{\delta}, \delta)$ varying within the fixed polytope β if matrices $P = P^T, L_1$, and L_2 can be found such that

$$\Psi = \begin{bmatrix} A_{a1}{}'P + PA_{a1} & PA_{a2} \\ A_{a2}{}'P & 0 \end{bmatrix}, \tag{3.80}$$

$$\Psi + L_2 C_{a2} + C_{a2}{}'L_2{}' < 0, \tag{3.81}$$

and

$$P + L_1 C_{a1} + C_{a1}{}'L_1{}' > 0 \tag{3.82}$$

are true at the vertices of β. In this case, the function,

$$v(x, \Theta_0(\delta)) = x(t)^T \begin{bmatrix} I \\ \Theta_0(\delta) \end{bmatrix}^T P \begin{bmatrix} I \\ \Theta_0(\delta) \end{bmatrix} x(t), \tag{3.83}$$

is a valid Lyapunov function for the system.

The proof of criteria in the form listed above can be found in [39], which also presents similar criteria for linearly parameter dependent systems. For more details on methods for transforming bilinear or quadratic matrix inequalities to affine LMI's, refer to [22].

As mentioned in Chapter 2, the selection of π_1, and thus $\Theta_0(\delta)$, is not unique. However, the manner in which $\Theta_0(\delta)$ is implemented into the stability analysis criteria is such that its composition affects the method's performance. Firstly, it is important that any parameters with bounded rates are included in the formulation of $\Theta_0(\delta)$. Since the rate of $\Theta_0(\delta)$ is the only rate considered in the LMI criteria, any parameters not included in its composition are assumed by the LMIs to vary arbitrarily fast. On the other hand, increasing the dimensions of $\Theta_0(\delta)$ also increases the dimensions of the decision matrices P, L_1, and L_2, rendering the feasibility problem more computationally costly. In addition to the example that is provided in the next section, details and examples on selecting $\Theta_0(\delta)$ in an adequate and efficient fashion can be found in [11].

Note that, despite the different form of the LMI conditions, quadratic stability and affinely parameter dependent Lyapunov functions are accounted for in the criteria described in the present section. In Equation 3.83, with P taking the form of Equation 3.75, the Lyapunov function becomes affinely parameter dependent if $P_2 = 0$. Moreover, if $P_2 = P_1 = 0$, P becomes a constant and the criteria test for quadratic stability [11]. In the general case where P_2 and P_1 are both non-zero, Equation 3.83 is referred to as a biquadratic Lyapunov function due to its quadratic dependence on the state and the uncertain parameters.

3.3.3 Simple Numerical Example for LMI Stability Analysis

This section uses a simple mechanical system as an example to display some of the properties of the modeling and stability analysis techniques presented in the previous and current chapter, respectively.

Consider the zero input spring-mass-damper system portrayed in Figure 3.1 described by the linear differential equation,

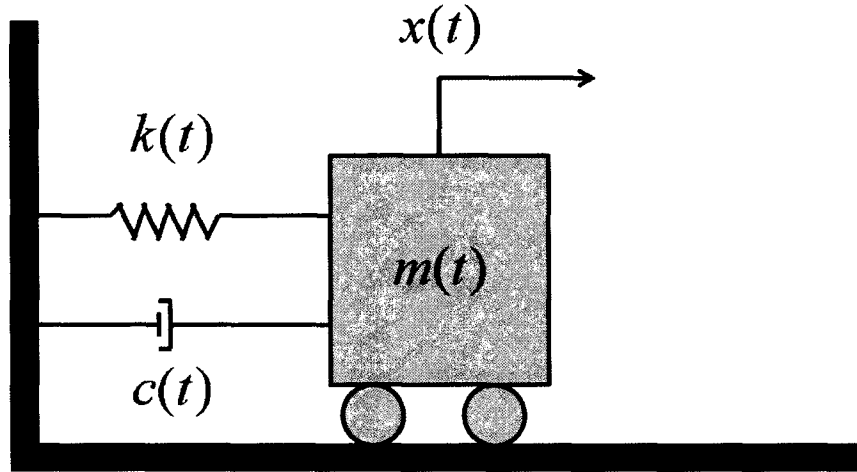$$m(t)\ddot{x}(t) + c(t)\dot{x}(t) + k(t)x(t) = 0. \tag{3.84}$$

Figure 3.1: Time-Varying Spring-Mass-Damper System

This system can be expressed in state-space form used throughout the current chapter as

$$E(p(t))\dot{x} = A(p(t))x, \tag{3.85}$$

where

$$x = \begin{bmatrix} x \\ \dot{x} \end{bmatrix}, \tag{3.86}$$

$$p(t) = \begin{bmatrix} k(t) \\ c(t) \\ m(t) \end{bmatrix}, \tag{3.87}$$

$$A(p(t)) = \begin{bmatrix} 0 & 1 \\ -k(t) & -c(t) \end{bmatrix}, \tag{3.88}$$

and

$$E(p(t)) = \begin{bmatrix} 1 & 0 \\ 0 & m(t) \end{bmatrix}. \tag{3.89}$$

Alternatively, by pre-multiplying both sides by $E(p(t))^{-1}$, Equation 3.83 can be recast in the form,

$$\dot{x} = \hat{A}(p(t))x, \tag{3.90}$$

where

$$\hat{A}(p(t)) = E(p(t))^{-1}A(p(t)) = \begin{bmatrix} 0 & 1 \\ -\frac{k(t)}{m(t)} & -\frac{c(t)}{m(t)} \end{bmatrix}. \tag{3.91}$$

The latter representation (Equation 3.90) is used in this section where it is necessary to discuss the techniques involving higher-order parameter dependence.

From the preceding equation, it is obvious that this system behaves as a parameter dependent system. In this case, it is most convenient to use the parameter dependent system model to map the system to a polytopic model as shown in Figure 2.4. Therefore, the system (Equation 3.85) is first modeled as affinely parameter dependent using the form of Equations 3.55 and 3.56 where $A(p)$ comprises the matrices

$$A_0 = \begin{bmatrix} 0 & 1 \\ 0 & 0 \end{bmatrix}, \quad A_k = \begin{bmatrix} 0 & 0 \\ -1 & 0 \end{bmatrix}, \quad A_c = \begin{bmatrix} 0 & 0 \\ 0 & -1 \end{bmatrix}, \quad A_m = \begin{bmatrix} 0 & 0 \\ 0 & 0 \end{bmatrix}, \tag{3.92}$$

and $E(p)$ comprises the matrices

$$E_0 = \begin{bmatrix} 1 & 0 \\ 0 & 0 \end{bmatrix}, \quad E_c = E_k = \begin{bmatrix} 0 & 0 \\ 0 & 0 \end{bmatrix}, \quad E_m = \begin{bmatrix} 0 & 0 \\ 0 & 1 \end{bmatrix}. \tag{3.93}$$

Further, the parameters vary such that

$$k(t) \in \left[\, \underline{k}, \overline{k} \,\right], \quad c(t) \in \left[\, \underline{c}, \overline{c} \,\right], \quad m(t) \in \left[\, \underline{m}, \overline{m} \,\right], \tag{3.94}$$

and

$$\underline{k} \leq \dot{k}(t) \leq \overline{\dot{k}}, \quad \underline{\dot{c}} \leq \dot{c}(t) \leq \overline{\dot{c}}, \quad \underline{\dot{m}} \leq \dot{m}(t) \leq \overline{\dot{m}}, \tag{3.95}$$

thus creating a convex parameter region with 64 vertices.

To transform this system into a polytopic model, the rate boundaries in Equation 3.95 are ignored, leaving a system defined by the 8 vertices of the parameter ranges. It is readily observed that $A(t)$ varies within the four-sided polytope defined by

$$A(t) \in \text{Co} \left(\begin{bmatrix} 0 & 1 \\ -\underline{k}(t) & -\underline{c}(t) \end{bmatrix}, \begin{bmatrix} 0 & 1 \\ -\underline{k}(t) & -\overline{c}(t) \end{bmatrix}, \begin{bmatrix} 0 & 1 \\ -\overline{k}(t) & -\underline{c}(t) \end{bmatrix}, \begin{bmatrix} 0 & 1 \\ -\overline{k}(t) & -\overline{c}(t) \end{bmatrix} \right), \tag{3.96}$$

and $E(t)$ varies within

$$E(t) \in \text{Co} \left(\begin{bmatrix} 1 & 0 \\ 0 & \underline{m}(t) \end{bmatrix}, \begin{bmatrix} 1 & 0 \\ 0 & \overline{m}(t) \end{bmatrix} \right). \tag{3.97}$$

From this information, the polytopic system model is created in the form of Equations 2.17, 2.18, and 2.19 or Equations 3.44 through 3.47.

To create the higher-order parameter dependent model, the system takes the form

of Equations 3.90 and 3.91. The relevant uncertain parameters become

$$p(t) = \boldsymbol{\delta}(t) = \begin{bmatrix} \delta_1(t) \\ \delta_2(t) \\ \delta_3(t) \end{bmatrix} = \begin{bmatrix} k(t) \\ c(t) \\ \frac{1}{m(t)} \end{bmatrix}. \tag{3.98}$$

Examining the system in terms of these parameters,

$$\dot{x} = \hat{A}(p(t))x = \begin{bmatrix} 0 & 1 \\ -\delta_1(t)\delta_3(t) & -\delta_2(t)\delta_3(t) \end{bmatrix} \begin{bmatrix} x_1 \\ x_2 \end{bmatrix}, \tag{3.99}$$

recall that the system must be expressed as shown in Equations 2.29, 2.30, and 2.31 in the

form

$$\hat{A}(p(t))x = \sum_{i=0}^{q} \hat{A}_i \pi_i. \tag{3.100}$$

Letting $\pi_0 = x$, $\hat{A}_0$ becomes

$$\hat{A}_0 = \begin{bmatrix} 0 & 1 \\ 0 & 0 \end{bmatrix} \tag{3.101}$$

to represent the parameter independent part of the system. The first auxiliary variable is

chosen as

$$\pi_1 = \begin{bmatrix} \delta_1(t)x_1 \\ \delta_2(t)x_2 \\ \delta_3(t)x_1 \end{bmatrix} \tag{3.102}$$

to reflect the necessary combinations of parameters and state variables while making sure

to include any parameters with bounded rates so that they appear in $\Theta_0(\boldsymbol{\delta})$. Given

Equation 3.102, $\hat{A}_1$ becomes

$$\hat{A}_1 = \begin{bmatrix} 0 & 0 & 0 \\ 0 & 0 & 0 \end{bmatrix}, \qquad (3.103)$$

reflecting that there are no first order parameter dependent terms in the system. The second auxiliary variable is defined

$$\pi_2 = \begin{bmatrix} \delta_1(t)\delta_3(t)x_1 \\ \delta_2(t)\delta_3(t)x_2 \end{bmatrix} \qquad (3.104)$$

to resemble the parameter dependent terms in Equation 3.99. Thus, $\hat{A}_2$ now becomes

$$\hat{A}_2 = \begin{bmatrix} 0 & 0 \\ -1 & -1 \end{bmatrix}. \qquad (3.105)$$

Substituting into Equation 3.100 yields

$$\hat{A}(p(t))x = \hat{A}_0\pi_0 + \hat{A}_1\pi_1 + \hat{A}_2\pi_2 \qquad (3.106)$$

$$= \begin{bmatrix} 0 & 1 \\ 0 & 0 \end{bmatrix}\begin{bmatrix} x_1 \\ x_2 \end{bmatrix} + \begin{bmatrix} 0 & 0 & 0 \\ 0 & 0 & 0 \end{bmatrix}\begin{bmatrix} \delta_1(t)x_1 \\ \delta_2(t)x_2 \\ \delta_3(t)x_1 \end{bmatrix} + \begin{bmatrix} 0 & 0 \\ -1 & -1 \end{bmatrix}\begin{bmatrix} \delta_1(t)\delta_3(t)x_1 \\ \delta_2(t)\delta_3(t)x_2 \end{bmatrix}$$

$$= \begin{bmatrix} 0 & 1 \\ -\delta_1(t)\delta_3(t) & -\delta_2(t)\delta_3(t) \end{bmatrix}\begin{bmatrix} x_1 \\ x_2 \end{bmatrix},$$

which verifies that this model is an accurate representation of the original system. Using Equation 2.30, the auxiliary variables are related such that

$$\pi_1 = \Theta_0(\delta)\pi_0 \qquad (3.107)$$

and

$$\pi_2 = \Theta_1(\delta)\pi_1. \qquad (3.108)$$

These relationships yield affine parameter matrices of

$$\Theta_0(\delta) = \begin{bmatrix} \delta_1(t) & 0 \\ 0 & \delta_2(t) \\ \delta_3(t) & 0 \end{bmatrix} \tag{3.109}$$

and

$$\Theta_1(\delta) = \begin{bmatrix} \delta_3(t) & 0 \\ 0 & \delta_3(t) \end{bmatrix}. \tag{3.110}$$

Next, the spring-mass-damper system will be used as a numerical example to explore the usefulness of the preceding modeling methods and the stability analysis criteria of Chapter 3 for various combinations of uncertain parameters and time-varying behavior. The analysis is performed by creating stability envelopes for each combination and each method. The axes show the percentage that the parameters can vary from the nominal. If a given point (x, y) is colored, it means that the stability criteria were found infeasible for the uncertain parameter vector,

$$p = \begin{bmatrix} p_x \\ p_y \end{bmatrix}, \tag{3.111}$$

ranging such that

$$p_x \in \left[p_{x_0}, \left(p_{x_0} + \frac{x}{100} p_{x_0} \right) \right] \tag{3.112}$$

and

$$p_y \in \left[p_{y_0}, \left(p_{y_0} + \frac{y}{100} p_{y_0} \right) \right]. \tag{3.113}$$

On the other hand, if a point (x, y) on the stability envelope is left unmarked, it means that the LMI stability conditions were found feasible for uncertain parameter vector

shown above. To visualize this test, for any point, (x, y), on the graph, the criteria are simultaneously testing parameter percentage variations at the vertices of the rectangle defined by

$$(x, y) = \left(\Delta p_x\% , \Delta p_y\%\right) \in Co\{(0,0), (x, 0), (0, y), (x, y)\}. \tag{3.114}$$

For a simple example, consider the first numerical test case below.

For all of the cases that follow, the nominal values assigned to the mass, damping, and stiffness are $m_0 = 1$, $c_0 = 2$, and $k_0 = 3$, respectively.

The first and simplest case holds the mass constant at its nominal value while the stiffness and damping coefficients, k and c, respectively, are uncertain but time-invariant. Using time-invariant stability criteria on the system matrix for this case, it is readily observed that for the eigenvalues to be negatively real valued, the conditions $k > 0$ and $c > 0$ must hold. These analytic findings are supported by a Monte Carlo analysis from [1] along with analysis performed using the three LMI methods from this chapter (Figure 3.2).

To analyze these plots, start at the nominal point, $(x, y) = (0,0)$, and pick a point on the graph. Consider, for example, the point $(x, y) = (50,100)$. By forming the rectangle outlined in Equation 3.114 and obtaining the parameter ranges using Equations 3.112 and 3.113, it is apparent that this point corresponds with the parameter vector

$$p = \begin{bmatrix} p_x \\ p_y \end{bmatrix} = \begin{bmatrix} c \\ k \end{bmatrix} \in Co\{\begin{bmatrix} 2 \\ 3 \end{bmatrix}, \begin{bmatrix} 3 \\ 3 \end{bmatrix}, \begin{bmatrix} 2 \\ 6 \end{bmatrix}, \begin{bmatrix} 3 \\ 6 \end{bmatrix}\}. \tag{3.115}$$

The fact that this point is unmarked signifies that the stability criteria were found feasible

for these vertices of the parameter region, meaning that the system is stable for all values

in the region. Consider a second point, $(x, y) = (-125, 100)$. Using Equations 3.112,

3.113, and 3.114, this point corresponds with the parameter vector

$$p = \begin{bmatrix} p_x \\ p_y \end{bmatrix} = \begin{bmatrix} c \\ k \end{bmatrix} \in Co\left\{ \begin{bmatrix} 2 \\ 3 \end{bmatrix}, \begin{bmatrix} -.5 \\ 3 \end{bmatrix}, \begin{bmatrix} 2 \\ 6 \end{bmatrix}, \begin{bmatrix} -.5 \\ 6 \end{bmatrix} \right\}. \tag{3.116}$$
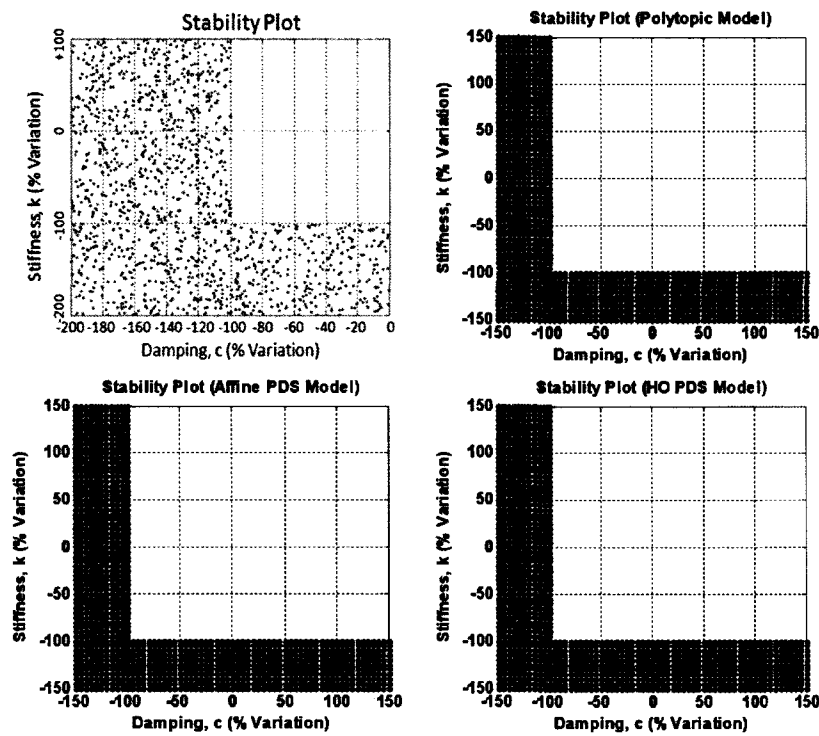

Figure 3.2: Stability Envelopes for LTI Spring-Mass-Damper

Since this point is marked red on the plot, the stability criteria were found infeasible for

the vertices of this parameter region. As stated previously, the results shown in Figure 3.2

support the analytical prediction for a LTI uncertain spring-mass-damper system.

Next, the quadratic stability analysis methods are tested. Recall that quadratic stability assumes that all uncertain parameters vary arbitrarily fast, and may therefore produce conservative results. In other words, the assumption of infinitely fast rates of variation may cause the LMI stability criteria to be found infeasible for regions of parameter values that would otherwise be stable under the system's actual operating conditions. The process for reading the quadratic stability plots is the same as the process for reading the plots from the LTI example.

Figures 3.3, 3.4, and 3.5 show the quadratic stability plots for different combinations of uncertain, time-varying stiffness, damping, and mass.

These plots illustrate the conservative nature of the quadratic stability criteria. Notice that for all three sets of uncertain parameters, the size of the rectangle that can be drawn from the origin, $(x, y) = (0,0)$, to another point without any of the vertices crossing into the red region is limited in size. This trait stems from the assumption that the parameters vary infinitely fast. By restricting the Lyapunov function to a function of the state variables but not the parameters, this assumption limits the size of the parameter regions for which the LMI criteria can be found simultaneously feasible at the vertices.
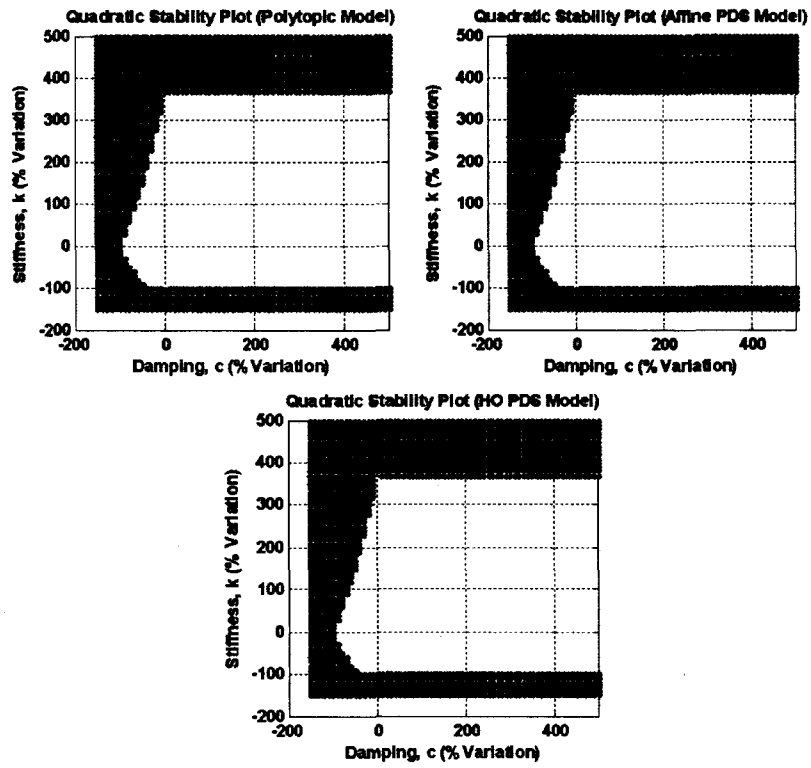
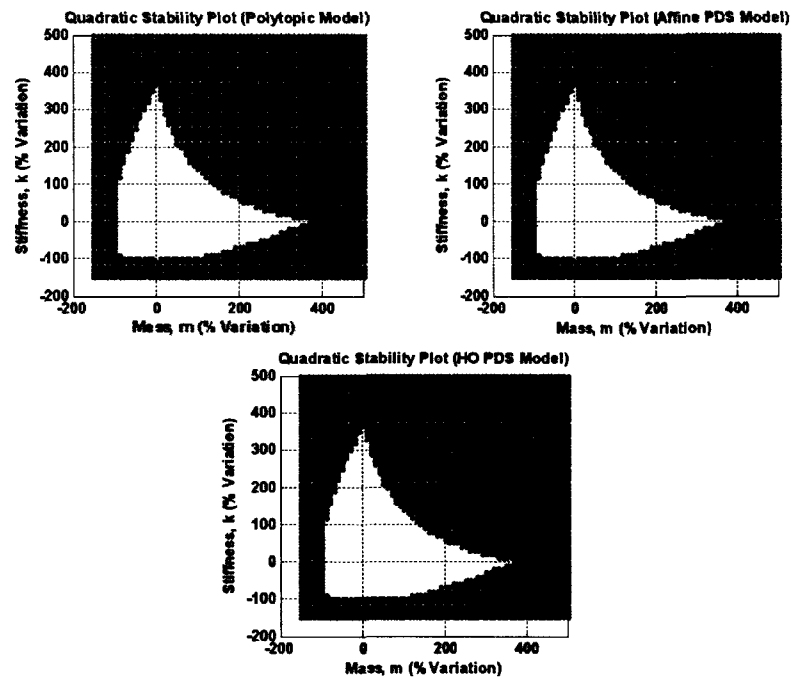**Figure 3.3: Quadratic Stability Plots for Uncertain Stiffness and Damping**

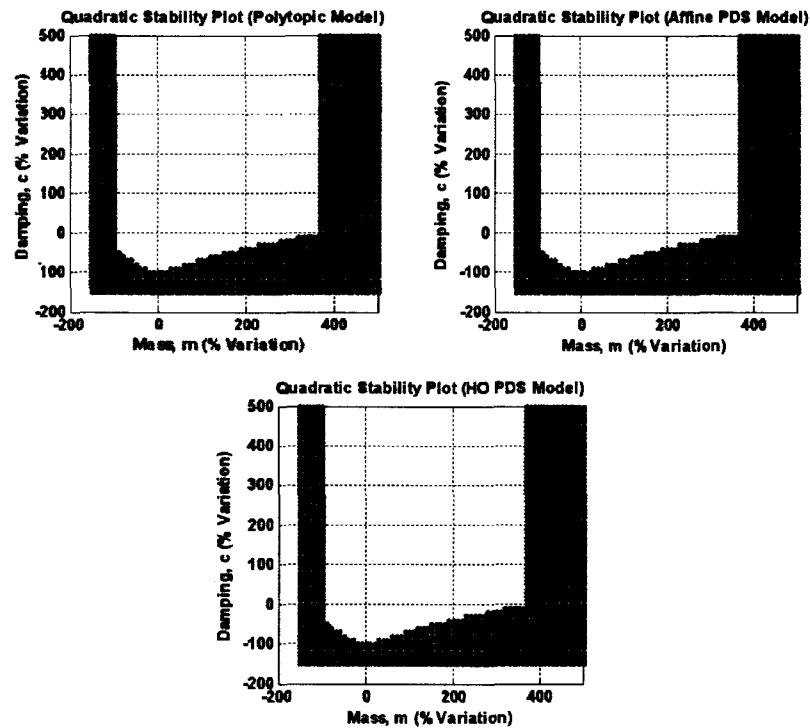**Figure 3.4: Quadratic Stability Plots for Uncertain Stiffness and Mass**

Figure 3.5: Quadratic Stability Plots for Uncertain Damping and Mass

Analyzing the stability of systems dependent on parameters with finite rates may be less

conservative than assuming the rates to be infinite. From the analysis in Section 3.3.1

[27], it is expected that decreasing bounds on the parameter rates will cause the stability

envelopes to approach those created with LTI stability criteria. Recall that polytopic

modeling does not allow for the incorporation of bounds on the parameter rates.

Therefore, the analysis will heretofore be limited to parameter dependent system models.

A second higher-order model is included with the limitation that the Lyapunov function

must be affinely parameter dependent (i.e. $P_2 = 0$ in Equation 3.75). The higher-order

model cases are labeled 'Q1' and 'Q2,' for affine and biquadratic parameter dependent

Lyapunov functions, respectively. (The terms 'Q1' and 'Q2', presented in [11], have

since been abandoned but are useful here to differentiate the higher-order plots from one

another.) In the figures that follow, the different colors representing stability envelopes corresponding to different bounds on the absolute value of the parameters' rate of variation. Note that a parameter region found infeasible for a given rate bound is also infeasible for any faster bound. Therefore, the envelopes for slower bounds have been plotted over top of the more conservative envelopes resulting from faster bounds. As expected, slower rate bounds yield less conservative stability envelopes that begin to resemble the results of the LTI stability criteria from Figure 3.2.
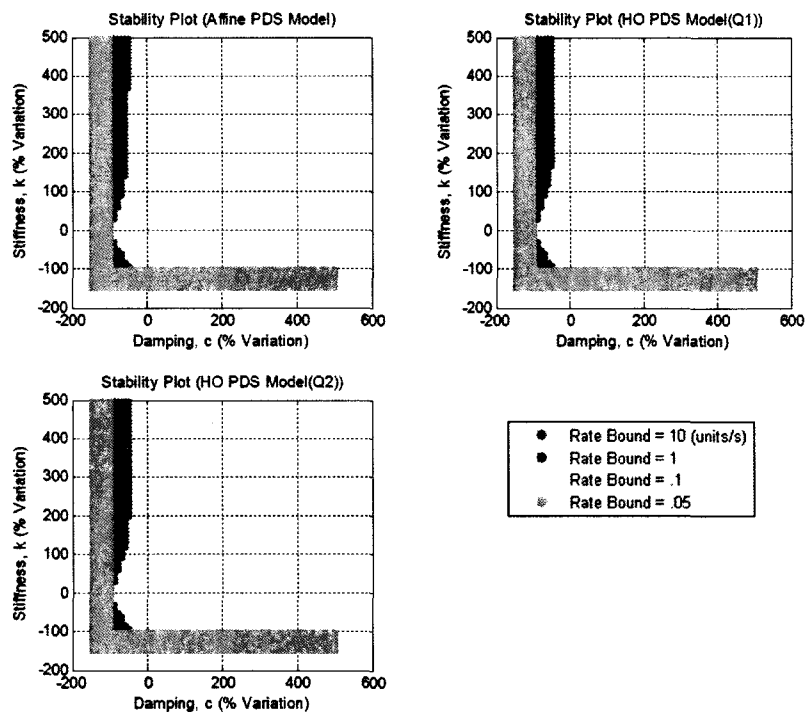

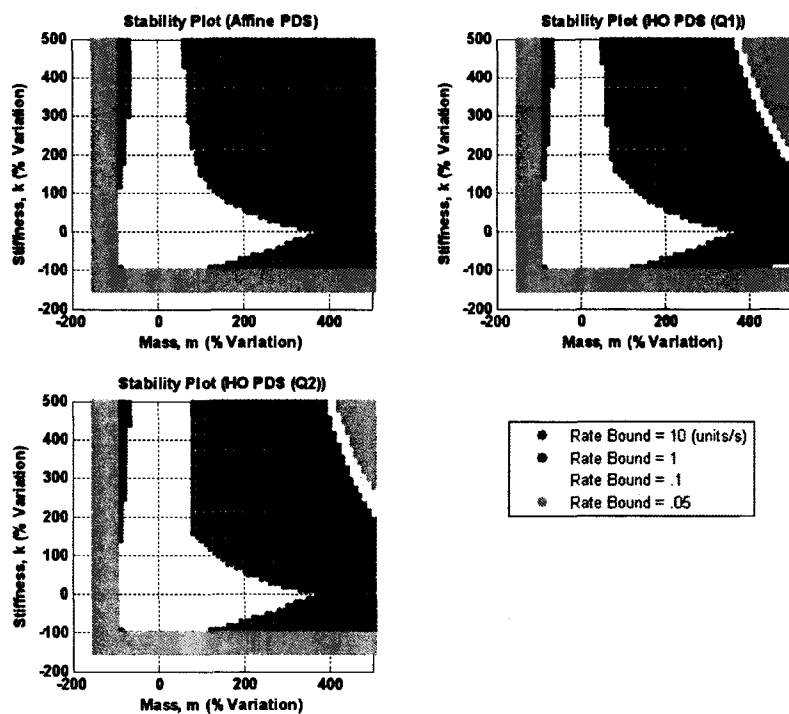**Figure 3.6: Stability Plots for Uncertain, Time-Varying Stiffness and Damping**

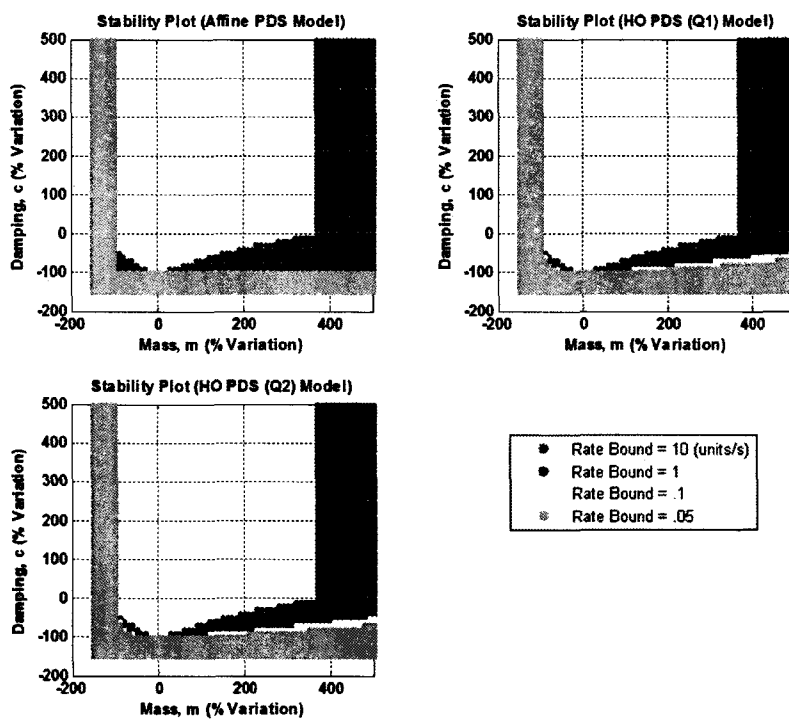**Figure 3.7: Stability Plots for Uncertain, Time-Varying Stiffness and Mass**

Figure 3.8: Stability Plots for Uncertain, Time-Varying Damping and Mass

These plots also begin to show certain differences in the performance of the various methods. In Figures 3.7 and 3.8, the cases where mass was time-varying, the criteria for the affine model appear to be less conservative than the criteria for the higher-order parameter dependent model. This occurs because in order to use the higher-order system model, the mass parameter, m, must be inversed (as shown in Equations 3.88 and 3.95), requiring the use of interval arithmetic to determine the bounds on the new parameter's range and rate. On the other hand, the mass needs not to be inversed for use in the affine system model. The performance of the affine and higher-order PDS models will be compared further in the case study in Chapter 5.

4 Relative Stability of Linear Time-Varying Systems

This chapter provides a review of gain and phase margin concepts and how they are typically used with time-invariant systems. Subsequently, methods for incorporating gain and phase margin into the previously described LMI stability analysis criteria are introduced in the interest of analyzing the relative stability for time-varying systems.

4.1 Relative Stability for Time-Invariant Systems

Relative stability is a design specification quantifying the amount of change that a system or its parameters can withstand before it becomes unstable [17]. Like stability, as presented in Chapter 3, this quantity is most readily evaluated using the system transfer functions.

Recall from Chapter 2 that a transfer function is the expression defining the relationship between the input and the output of a control system. Consider Figure 4.1, a generalized block diagram of a transfer function where U is the input, Y is the output, and G and H are transfer functions of individual system components [17].
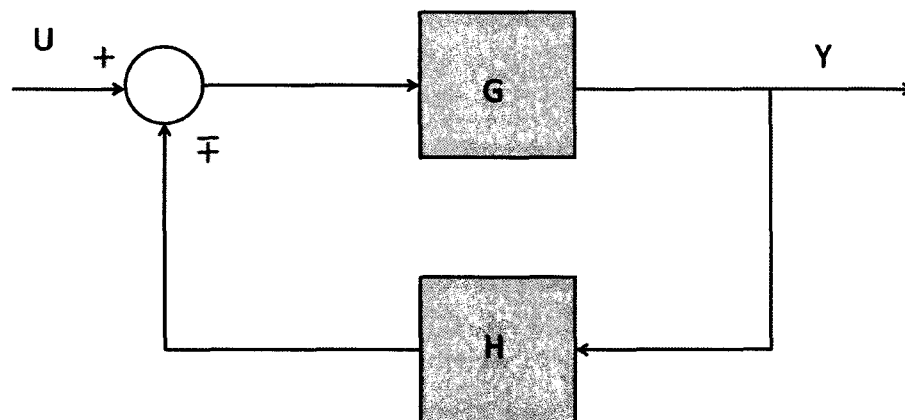

Figure 4.1: Block Diagram of Control System Transfer Function

Systems where H is non-zero are known as closed loop systems because the control

action is dependent on the output to some degree. The '∓' at the summing block

indicates the option for either negative or positive feedback. Systems designed for

stability typically utilize negative feedback. The transfer function of the closed loop

system takes the form

$$T_{cl}(s) = \frac{Y(s)}{U(s)} = \frac{G(s)}{1 \pm G(s)H(s)}. \tag{4.1}$$

Chapter 2 states that a system becomes unstable when its transfer function value

approaches infinity. For the general transfer function shown above, this occurs when

$$1 \pm G(s)H(s) = 0. \tag{4.2}$$

Quantifying relative stability, therefore, involves analyzing the open loop transfer

function, $G(s)H(s)$, to determine how much it can vary before this occurs [17][18].

For example, in a negative feedback system, Equation 4.2 is true when

$G(s)H(s) = -1$. Recall that transfer functions are functions of $s = \sigma + j\omega$ and

therefore take on complex values, which can be plotted in the "s-plane." Subsequently,

the value can be expressed as a combination of the magnitude and phase angle of the

vector from the origin to the point (Figure 4.2), which are defined

$$|p| = \sqrt{a^2 + b^2} \tag{4.3}$$

and

$$\tan(\phi_p) = \left(\frac{b}{a}\right), \tag{4.4}$$

respectively, for a complex number $p = a + jb$.
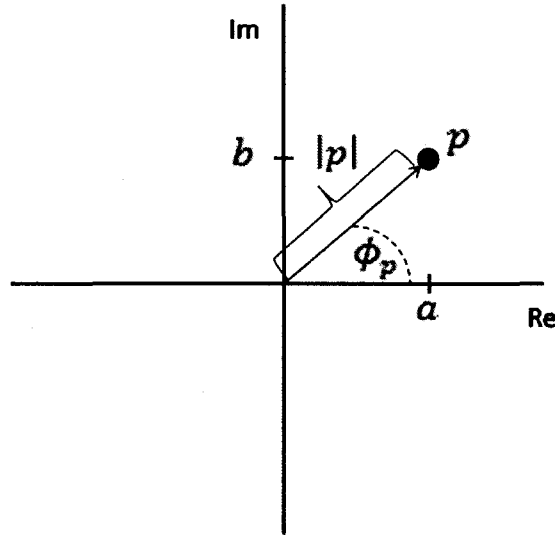
Figure 4.2: Magnitude and Phase Angle of a Complex Number

The gain and phase margins are determined by evaluating the magnitude and

phase of the open loop transfer function, $G(s)H(s)$, over a range of frequencies. This

technique is known as finding the transfer function's frequency response and is

performed by letting $s = j\omega$. Consider again the example of a negative feedback

system. $G(s)H(s) = -1$ corresponds to $|G(s)H(s)| = 1$ and $\phi_{GH} = -180° \pm n360°$,

where n is any integer. Therefore, gain margin is defined as

$$gain\ margin = \frac{1}{|G(s)H(s)|}\bigg|_{s=j\omega_\pi},$$ (4.5)

where ω_π is the frequency (or frequencies) at which $\phi_{GH} = -180° \pm n360°$. Likewise,

phase margin is defined as

$$phase\ margin = 180° + \phi_{GH}|_{s=j\omega_1}, \tag{4.6}$$

where ω_1 is the frequency (or frequencies) at which $|G(s)H(s)| = 1$ [17].

The gain and phase margin of a LTI system can be designed for and analyzed using one of the graphical methods mentioned in beginning of Chapter 3, including Nyquist, Nichols, root locus, and Bode plots. For detailed discussion and examples of these graphical methods, refer to [18].

4.2 Relative Stability for Time-Varying Systems

As stated in Chapter 3 and in the previous section, frequency response methods are typically associated with time-invariant systems. Like stability analysis, evaluating the relative stability of systems in industrial applications is often accomplished with frozen time analysis under the assumption that the system at hand is sufficiently slowly varying. Quadratic stability margins [27] and non-linear techniques like absolute stability and circle criterion [40] are tools that can determine the margins for time-varying systems. However, these methods may be conservative for linear systems with bounded rates of variation.

The goal of stability analysis in industry is often to ensure a certain level of robustness against parameter uncertainty for a designed control system. Stability margins tell the engineer(s) if a new controller must be designed or if the system meets the relative stability specifications. By imposing desired gain and phase margin requirements on the system models, the LMI criteria described and tested in Chapter 3 can determine if a designed system meets margin requirements for time-varying parameter uncertainty by taking advantage of knowledge on the system's parameter ranges and rates of variation.

4.2.1 Gain Margin Testing for Time-Varying Systems

Since the aforementioned LMI criteria make use of state space system models, it is important to understand how gain margin, described in the previous section for the frequency domain, appears in time domain models. Recall the general block diagram from Figure 4.1, but let G and H be modeled in the time domain as the state space systems

$$\dot{x}_G(t) = A_G(t)x_G(t) + B_G(t)u_G(t) \tag{4.7}$$

$$y_G(t) = C_G(t)x_G(t) + D_G(t)u_G(t) \tag{4.8}$$

and

$$\dot{x}_H(t) = A_H(t)x_H(t) + B_H(t)u_H(t) \tag{4.9}$$

$$y_H(t) = C_H(t)x_H(t) + D_H(t)u_H(t). \tag{4.10}$$

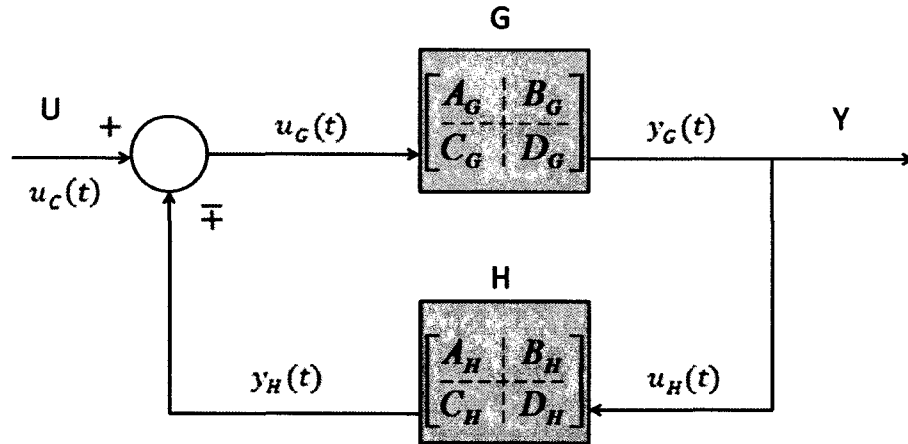Figure 4.3 is an updated block diagram of this system.

Figure 4.3: Block Diagram of Control System Transfer Function in State Space Form

From this diagram, it is obvious that the input to the feedback transfer function, H, of the system is equivalent to the output of the forward transfer function, G, or

$$u_H(t) = y_G(t). \tag{4.11}$$

Furthermore, the input to G is expressed

$$u_G(t) = u_C(t) \mp y_H(t). \tag{4.12}$$

By substituting these equations with Equations 4.7 through 4.10, the equations for the closed loop system become

$$\dot{x}_{CL} = \begin{bmatrix} A_G \mp B_G \Delta^{-1} D_H C_G & \mp B_G \Delta^{-1} C_H \\ B_H C_G \mp B_H D_G \Delta^{-1} D_H C_G & A_H \mp B_H D_G \Delta^{-1} C_H \end{bmatrix} x_{CL} + \begin{bmatrix} B_G \Delta^{-1} \\ B_H D_G \Delta^{-1} \end{bmatrix} u_C \tag{4.13}$$

$$y_{CL} = y_G = [C_G \mp D_G \Delta^{-1} D_H C_G \quad \mp D_G \Delta^{-1} C_H] x_{CL} + [D_G \Delta^{-1}] u_C \tag{4.14}$$

where

$$x_{CL}(t) = \begin{bmatrix} x_G(t) \\ x_H(t) \end{bmatrix} \tag{4.15}$$

$$\Delta^{-1} = (I + D_H(t) D_G(t))^{-1}. \tag{4.16}$$

In this regard, note that the matrices in Equations 4.13 and 4.14 are still time-varying, but the time dependence is not explicitly shown in order to simplify the notation. Referring back to the block diagram for LTI systems in Figure 4.1, note that if a desired gain margin, K, is placed in the system, as shown in Figure 4.4,
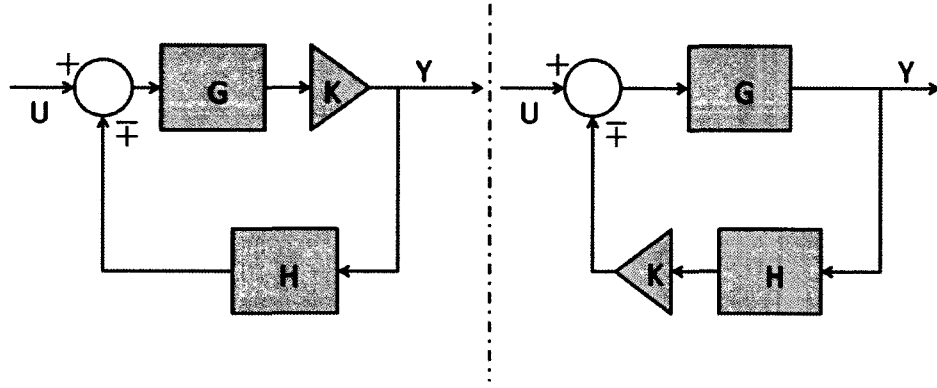
Figure 4.4: Block Diagram of Transfer Function Control System with Gain

the system transfer function for the left side becomes

$$T_{CL} = \frac{KG}{1 \pm KGH},$$ (4.17)

and the transfer function for the right side becomes

$$T_{CL} = \frac{G}{1 \pm KGH}.$$ (4.18)

The denominators for these transfer functions are identical. Therefore, from a stability standpoint, it does not matter where in the system the gain margin is multiplied.

Multiplying the output equations in the state space representation of the system yields similar results. If the gain margin, K, is incorporated into system G, the closed loop system becomes

$$\dot{x}_{CL} = \begin{bmatrix} A_G \mp KB_G\Delta^{-1}D_HC_G & \mp B_G\Delta^{-1}C_H \\ KB_HC_G \mp K^2B_HD_G\Delta^{-1}D_HC_G & A_H \mp KB_HD_G\Delta^{-1}C_H \end{bmatrix} x_{CL} + \begin{bmatrix} B_G\Delta^{-1} \\ KB_HD_G\Delta^{-1} \end{bmatrix} u_C$$

(4.19)

$$y_{CL} = Ky_G = [KC_G \mp K^2D_G\Delta^{-1}D_HC_G \quad \mp KD_G\Delta^{-1}C_H]x_{CL} + [KD_G\Delta^{-1}]u_C.$$ (4.20)

If K multiplies the output of system H, the system becomes

$$\dot{x}_{CL} = \begin{bmatrix} A_G \mp KB_G\Delta^{-1}D_HC_G & \mp KB_G\Delta^{-1}C_H \\ B_HC_G \mp KB_HD_G\Delta^{-1}D_HC_G & A_H \mp KB_HD_G\Delta^{-1}C_H \end{bmatrix} x_{CL} + \begin{bmatrix} B_G\Delta^{-1} \\ B_HD_G\Delta^{-1} \end{bmatrix} u_C$$

(4.21)

$$y_{CL} = y_G = [C_G \mp KD_G\Delta^{-1}D_HC_G \quad \mp KD_G\Delta^{-1}C_H]x_{CL} + [D_G\Delta^{-1}]u_C.$$ (4.22)

For both systems,

$$\Delta^{-1} = (I + KD_H(t)D_G(t))^{-1}.$$ (4.23)

Noting the differences in the system matrices above, it must be determined whether they have equivalent stability characteristics with respect to the criteria used for time-varying systems. To simplify the differences, realize that the system matrices of the above systems resemble the matrices

$$A_{CLG} = \begin{bmatrix} a & b \\ Kc & d \end{bmatrix}$$ (4.24)

and

$$A_{CLH} = \begin{bmatrix} a & Kb \\ c & d \end{bmatrix}.$$ (4.25)

Clearly, the eigenvalues of these two system matrices are the same even if a, b, c, and d are time-varying. This means that there is no combination of a, b, c, d, and K that will make the one of the systems (Equations 4.42 and 4.23) stable and the other instable according to the quadratic Lyapunov criteria in Equation 3.27. This statement is readily verified using Monte Carlo analysis to create several realizations of the systems with

random variables for the parameters [8]. Therefore, it can be concluded that even in the presence of time-varying parameters, it does not matter where the gain margin, K, is applied to the open loop.

Using this information, the desired gain margin, K, is applied to the system wherever it is most convenient. If the LMI stability criteria are found simultaneously feasible for the original system and the new system for a certain region of parameter rates and ranges, the original system has a gain margin of at least K for all parameter values within that region. In some cases, it may be desired to test for two gain margins simultaneously: a margin, K, for amplification and a margin, $1/K$, for attenuation. In this case, two new systems can be formed, one with each desired margin. If the LMI stability criteria from Chapter 3 are found simultaneously feasible for both systems, the original system has a "positive" and "negative" gain margin of at least K for all operating conditions described by the tested parameter region.

4.2.2   Phase Margin Testing for Time-Varying Systems

Phase angle is used to describe the relationship between a complex number's real and imaginary parts, as shown in Equation 4.3. Figure 4.5 shows the phase angle and related trigonometry for a complex number $p = a + jb$.
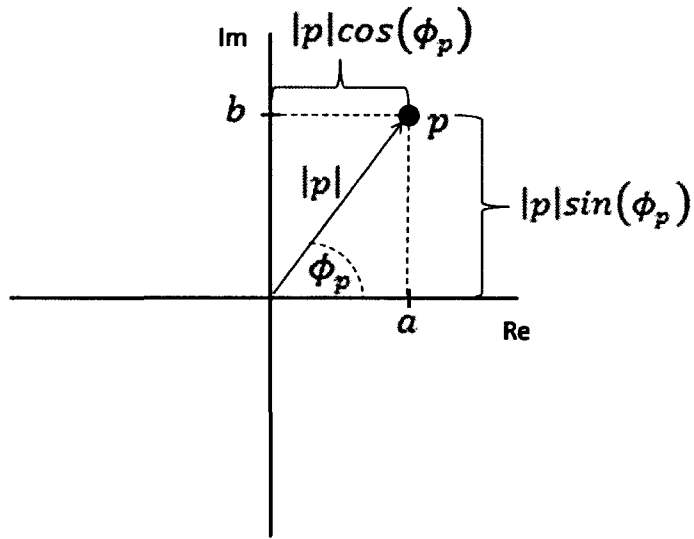
Figure 4.5: Phase Angle in the S- Plane

The relationships

$$a = |p|cos(\phi_p) \tag{4.26}$$

and

$$b = |p|sin(\phi_p) \tag{4.27}$$

provide an alternate expression for p in terms of its phase and magnitude,

$$p = |p|cos(\phi_p) + j|p|sin(\phi_p). \tag{4.28}$$

Recall, however, that the phase angle of a system originates from the frequency response technique, which is based on LTI transfer functions. Hence, an alternative tool will be used to measure the relative stability. Delay margin, as presented in [41] and described in the remainder of this section, is a viable substitute. To see the relationship

between time delay and phase angle, consider the representation of a time delay, τ, in the

s-domain,

$$L[f(t - \tau)] = e^{-\tau s}F(s). \tag{4.29}$$

In block diagram representation, the time delay above takes the form of Figure 4.6.
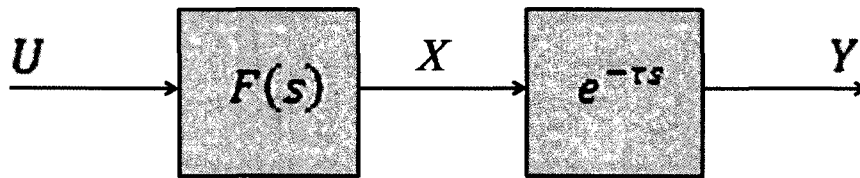
Figure 4.6: Block Diagram of Transfer Function with Delay

Consider that the frequency response technique evaluates the transfer functions at

$s = j\omega$, meaning that

$$e^{-\tau s} = e^{-\tau j\omega}. \tag{4.30}$$

Using Euler's formula [33],

$$e^{jy} = \cos(y) + j\sin(y), \tag{4.31}$$

the time delay can be expressed

$$e^{-\tau j\omega} = \cos(-\tau\omega) + j\sin(-\tau\omega). \tag{4.32}$$

Comparing Equations 4.28 and 4.32, the relationship between a time delay and phase

angle becomes

$$-\tau\omega_1 = \phi_d, \tag{4.33}$$

where ϕ_d is the phase change caused by the delay and ω_1 represents any frequency (in radians) where the magnitude is unity [41][42].

Control systems analysis software may require that the delay transfer function be represented by a transfer function other than an exponential function in order for the closed loop system matrix values to reflect the change. In this case, [41] presents methods for applying a so-called Padé approximation, a method for accurately approximating a function as a rational function of a finite order [43].

Specifically, Equation 4.30 can also be written as the nth-order Padé approximation,

$$e^{-\tau s}F(s) = \frac{1-p_1(\tau s)+p_2(\tau s)^2...p_n(\tau s)^n}{1+p_1(\tau s)+p_2(\tau s)^2...p_n(\tau s)^n}. \tag{4.34}$$

In the first order approximation,

$$e^{-\tau s}F(s) \sim \frac{1-p_1\tau s}{1+p_1\tau s}, \tag{4.35}$$

the delay margin, τ, can be isolated, making it simple to apply a desired margin [41]. This is accomplished by first representing the delay as an additive perturbation such that

$$\frac{1-p_1\tau s}{1+p_1\tau s} = 1 - D(s). \tag{4.36}$$

Figure 4.7 presents the general structure of this representation. From Equation 4.36, the transfer function, $D(s)$, is determined
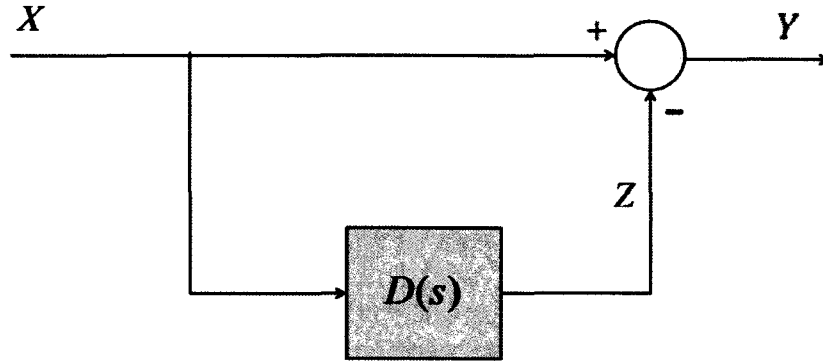
$$D(s) = \frac{-2p_1\tau s}{1+p_1\tau s}. \tag{4.37}$$

Figure 4.7: Block Diagram of Additive Perturbation

The selection of $p_1 = \frac{1}{2}$ gives

$$D(s) = \frac{\tau s}{1+\frac{\tau}{2}s}.$$ (4.38)

Rearranging $D(s)$ in terms of X and Z from Figure 4.7 yields

$$Z = \frac{\tau s}{1+\frac{\tau}{2}s}X \quad \Rightarrow \quad Z = \tau s\left(X - \frac{Z}{2}\right),$$ (4.39)

which is shown in block diagram form in Figure 4.8. This delay transfer function is then

applied to the open loop transfer function of the original time-varying system (Figure 4.3)

as shown in Figure 4.9.

Given a desired phase margin, Equation 4.33 yields the appropriate time delay, τ,

to include in the delay transfer function described above. However, due to the frequency

dependence in the expression, the process requires more calculation than the gain margin.
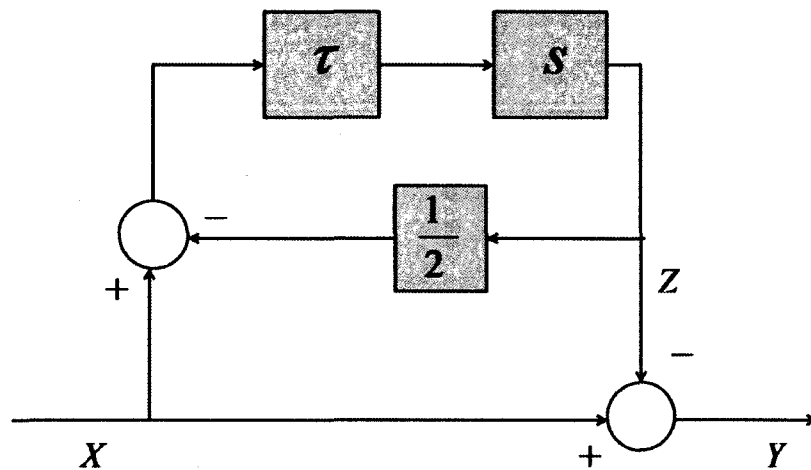
Figure 4.8: Block Diagram of First Order Padé Approximation of Delay Margin
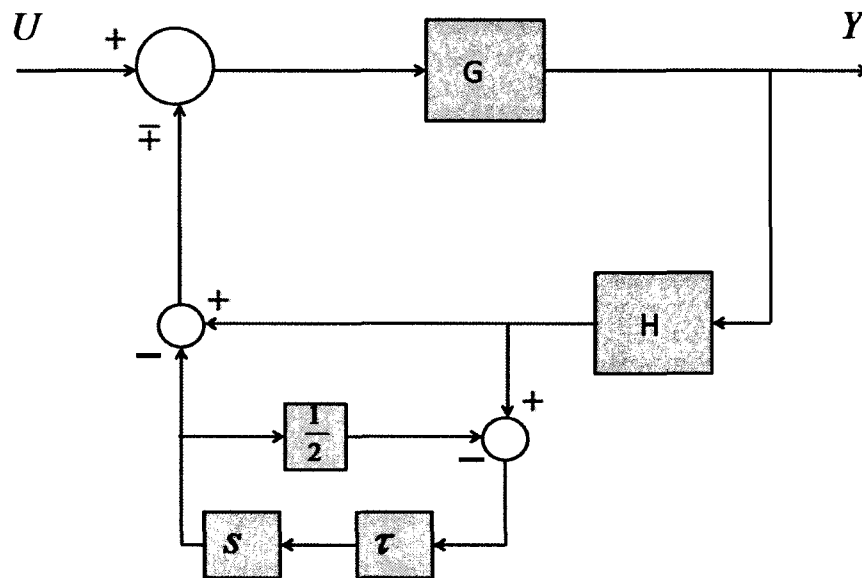
Figure 4.9: Application of Delay Margin Approximation to Transfer Function

To account for this dependence, LTI systems are formed at the vertices of the parameter ranges of the system being tested, and the phase margins of these vertex systems are obtained using methods mentioned in Section 4.1. The frequency, ω_1, for the smallest phase margin is determined for each vertex system. The slowest of these vertex frequencies is then used to calculate the appropriate time delay using the formula

$$\tau = \pm \frac{\phi_{test}}{\omega_1},$$
(4.40)

where ϕ_{test} is the desired phase margin in radians.

If the LMI criteria are feasible for the systems with the incorporated time delays, then the system has a phase margin, or the equivalent time-delay margin, of at least ϕ_{test} for all parameter ranges and rates tested.

Knowledge of the behavior of real life systems may dictate that only positive or negative delay margins be tested. For example, if a certain system is designed without any delay (i.e. $\tau = 0$ for the nominal case), it is susceptible only to a positive time delay (assuming it is a physically realizable system). Therefore, it is extraneous to test for a negative time-delay margin. In this case, the system has a phase margin of at least ϕ_{test} if the LMI criteria are found simultaneously feasible for the original system and the system with the positive time delay included.

5 Case Study: Time-Varying Stability and Robustness for Spacecraft

The many interesting case studies that could be used to evaluate and compare stability analysis methods for time-varying systems include, but are not limited to, a flexible manipulator [44], spring-mass-damper [11][13], a high-performance aircraft [34][41][45], a launch vehicle [14][46][47][48], and other high-performance machines [49]. This thesis presents a case study featuring the attitude control system for a launch vehicle modeled as a parameter dependent linear time-varying system.

The several different categories of launch vehicles range in complexity from missiles [48] and single-stage-to-orbit (SSTO) vehicles [46], to larger spacecraft with liquid fuel tanks [47] and/or multiple stages. In order to include time-varying parameters like the behavior of sloshing fuel [50] and a larger variety of operating conditions, this case study features a two-stage vehicle with solid and liquid fuel tanks, represented by the dynamics presented in [14].

The first section presents the assumptions that were made in the course of the analysis. This is followed by a section reviewing the relevant spacecraft dynamics. Subsequently, the system is analyzed using the parameter dependent LMI methods for time-varying stability analysis described in Chapter 3. First, stability envelopes for aerodynamic coefficient, thrust, slosh frequency, and slosh damping, are presented for the system at certain time-slices to compare the results from LMI methods to one another and to the results from frozen time analysis. Furthermore, rate bounds are added to examine how time-varying parameters affect the stability envelope. The time of flight is then

divided into overlapping time intervals to evaluate stability margin requirements for system model.

5.1 Assumptions

For a complex system like a spacecraft, it is necessary to make simplifying assumptions in order to efficiently use the stability analysis tools discussed in this thesis. First of all, the methods described thus far are valid for linear systems only. Therefore, the inherent non-linearities in the dynamics of the spacecraft are either treated as negligible or represented with linearized approximations in the equations of motion [1][5][14].

The system's six degrees of freedom (DOF) include rotation and translation in each of the roll, pitch, and yaw, axes. The roll, however, is typically directed by a non-linear controller that is separate from the attitude control system being examined in this case study. Further, it is assumed that the vehicle is quite close to symmetrical in the pitch and yaw axis (Figure 5.1), so a control system designed for the yaw axis will meet the same stability requirements in the pitch axis, and vice versa [1][5]. This simplification reduces the system to 2 DOF.

5.2 System Dynamics

Due to the assumptions in the previous section, the spacecraft can now be represented as a system of linear equations. These equations, presented in their entirety in [14], can be divided into rigid body dynamics, flex (bending) dynamics, and slosh dynamics.
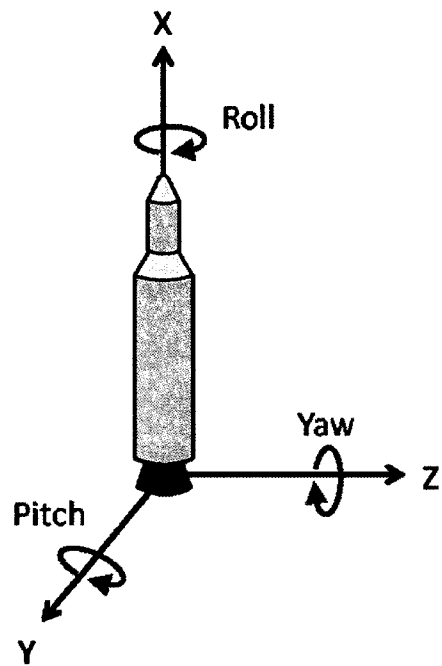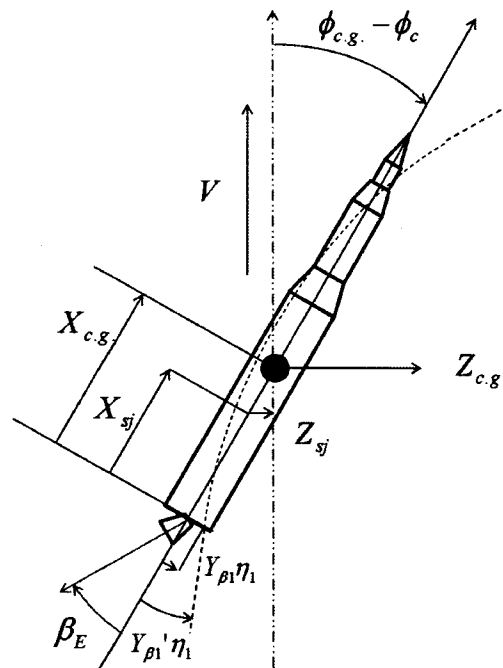
Figure 5.1: Spacecraft Coordinate Frame

Figure 5.2: Spacecraft Sign Conventions

Figure 5.2 shows the sign conventions for the equations of motion that will be presented in the remainder of the current section with variables as defined in the List of Variables [1][14]. Note that the 2 DOF in this depiction include translation in the Z-axis and rotation in the Y-axis.

Rigid body dynamics includes rigid rotation about the center of gravity and the rigid body translation of the center of gravity. Specifically,

$$\phi_{c.g.}s^2 = -c_1\alpha - c_2\beta_E - \frac{1}{I_{xx}}(X_{c.g}S_E + I_E)\beta_E s^2 + \frac{1}{I_{xx}}\sum_{j=1}^{n_s} m_{sj}(l_{sj}s^2 + k_3)Z_{sj}$$

(5.1)

and

$$Z_{c.g.}s^2 = k_7\alpha + k_4\beta_E + k_3\phi_{c.g.} + \frac{S_E}{M}\beta_E s^2 - \frac{1}{M}\sum_{j=1}^{n_s} m_{sj}Z_{sj}s^2.$$

(5.2)

Both kinds of rigid body motion depend on forces created by aerodynamic properties, gimbal angle (including the "tail-wags-dog" effect), thrust, drag, and sloshing fuel masses. Equations 5.1 and 5.2 are linked together by the equation,

$$\alpha = \left(\frac{V_w}{V}\right) + \phi_{c.g.} - \left(\frac{Z_{c.g.}s}{V}\right),$$

(5.3)

which expresses angle of attack in terms of attitude and translation.

Bending motion (Equation 5.4) depends on flexibility characteristics such as natural frequency, damping, and generalized mass in addition to the forces mentioned above for the rigid body dynamics. Specifically,

$$(s^2 + 2\zeta_{Bi}\omega_{Bi}s + \omega_{Bi}{}^2)M_i\eta_i = R'Y_{Bi}\beta_E + (S_E Y_{Bi} - I_E Y_{Bi}{}')\beta_E s^2 -$$

$$\sum_{j=1}^{n_s} m_{sj}Y_{sij}Z_{sj}s^2 + C_{Z\eta i}\alpha. \tag{5.4}$$

Each bending mode is represented by a separate equation. The inclusion of more bending modes in a model leads to an increase in model fidelity. However, this also leads to an increase in the size of the system. The number of modes included in an analysis ultimately depends on the required model fidelity, the vehicle's frequency spectrum, and the available computation tools [1].

The dynamics of sloshing fuel is described by an equation for each fuel tank being considered in the analysis. Specifically,

$$(s^2 + 2\zeta_{sj}\omega_{sj}s + \omega_{sj}{}^2)Z_{sj} = -Z_{c.g.}s^2 + (l_{sj}s^2 + k_3)\phi_{c.g.} - \sum_{i=1}^{n_b} Y_{sij}\eta_i s^2. \tag{5.5}$$

Similar to bending modes, the inclusion of more slosh masses (up to the true number) yields a higher fidelity model. As shown in Equations 5.1, 5.2, and 5.4, the slosh tanks with greater slosh masses have a larger effect on overall vehicle motion.

Equations 5.1 through 5.5 describe the overall motion of the spacecraft and collectively form the plant system. In addition to the plant, the control system includes a combination of other systems designed to regulate the spacecraft's attitude. Sensors on the body of the vehicle determine the attitude and attitude rate according to the equations

$$\phi_p = \phi_{c.g.} + \sum_{i=1}^{n_b} Y_{\phi i}{}'\eta_i \tag{5.6}$$

and

$$\dot{\phi}_{RG} = \phi_{c.g.}s + \sum_{i=1}^{n_b} Y_{\phi i}{}'\eta_i s, \tag{5.7}$$

respectively. It is apparent that sensor output only differs from plant output if bending

dynamics is included in the model. Note that, when convenient, the sensor equations can

be included as part of the plant's output equations.

Sensor output is filtered in order to attenuate the higher frequency bending modes

[1][16]. The filter output becomes the controller input. The controller is a proportional-

integral-derivative (PID) controller that outputs a gimbal command angle

$$\beta_{CMD} = K_i \int (\phi_p - \phi_c) + K_p(\phi_p - \phi_c) + K_d \dot{\phi}_{RG}. \tag{5.8}$$

The controller gains, K_i, K_p, and K_d, are designed using gain scheduling, a process that

involves optimizing a controller for specific design points throughout the time of flight

and linearly interpolating between these points to obtain gain values for any flight time

[1][18][44]. The command angle translates the gimbal angle via the dynamics of the

actuator. Figure 5.3 presents the basic structure of how the separate systems interact to
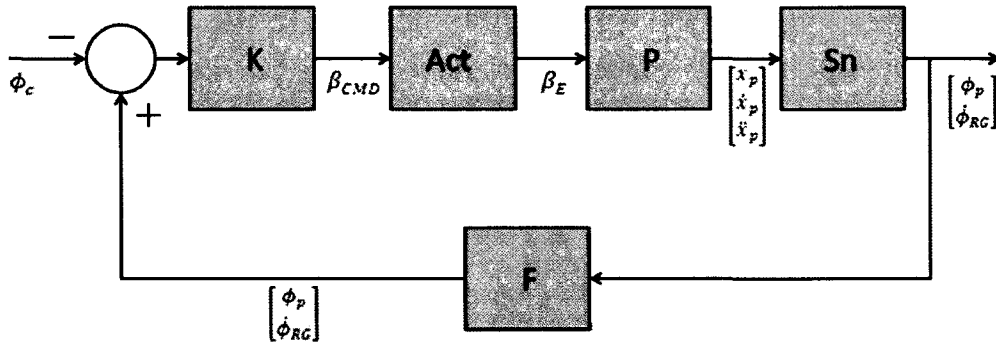
form the attitude control system.

Figure 5.3: Spacecraft Attitude Control System Block Diagram

After transforming each system into its state space representation, the process in

Equations 4.6 through 4.15 can be used to represent the system as one larger state space

model. With an understanding of the system's parameter dependence, the LMI stability criteria from Chapter 3 can evaluate the stability of the system subject to different sets of uncertain parameter ranges and rates.

5.3 Stability for a Rigid Spacecraft

In this section, the system is simplified to reduce the size of the model and enable faster computations. This simplification facilitates the stability analysis for several sets of uncertain parameters and operating conditions. Testing such large ranges of operating conditions yields stability envelopes for the different parameter combinations. These results are compared to the corresponding stability envelopes from frozen time analysis methods to quantify the LMI methods' conservativeness.

To reduce the size of the system, the bending dynamics is removed from the original model. From Equations 5.6 and 5.7, it is apparent that this enables the removal of the sensor system. More importantly, the flex filter is no longer needed to attenuate the effects of the bending motion. Finally, to further simplify the system model, the "tail-wags-dog" effect between the plant and the actuator is ignored. Figure 5.4 shows the reduced structure of the attitude control system.
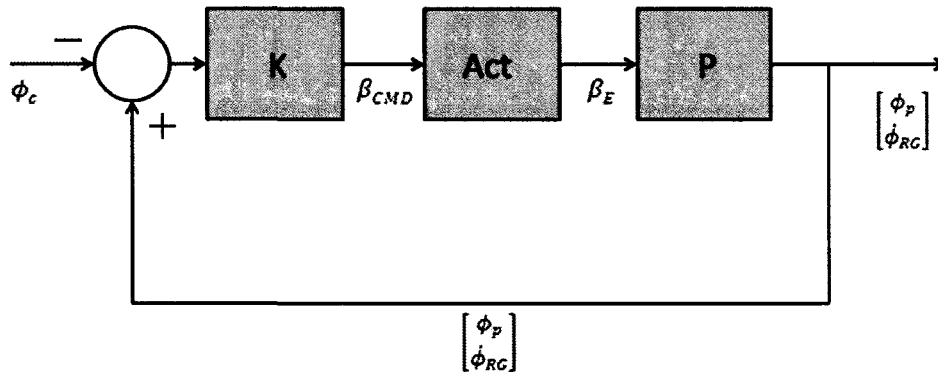

Figure 5.4: Simplified Attitude Control System Model

Given the state space models,

$$\dot{x}_p = A_p(\delta)x_p + B_p(\delta)\beta_E \tag{5.9}$$

$$y = C_p x_p + D_p \beta_E = C_p x_p, \tag{5.10}$$

$$\dot{x}_{act} = A_{act} x_{act} + B_{act} \beta_C \tag{5.11}$$

$$\beta_E = C_{act} x_{act} + D_{act} \beta_C = C_{act} x_{act}, \tag{5.12}$$

and

$$\dot{x}_K = A_K x_K + B_K y \tag{5.13}$$

$$\beta_C = C_K x_K + D_K y, \tag{5.14}$$

for the plant, actuator, and controller, respectively, the homogeneous closed-loop control

system becomes

$$\dot{x} = \begin{bmatrix} \dot{x}_p \\ \dot{x}_{act} \\ \dot{x}_K \end{bmatrix} = \begin{bmatrix} A_p(\delta) & B_p(\delta)C_{act} & 0 \\ B_{act}D_K C_p & A_{act} & B_{act}C_K \\ B_K C_p & 0 & A_K \end{bmatrix} \begin{bmatrix} x_p \\ x_{act} \\ x_K \end{bmatrix} = A(t)x(t). \tag{5.15}$$

Note that the parameter dependence in the system is limited to $A_p(\delta)$ and $B_p(\delta)$, and that

the system has been structured so the time-varying parameters are confined to two

adjacent block elements, simplifying the creation of the uncertain state space systems.

Using Equations 5.1 through 5.5 and the processes illustrated in the numerical example in

Chapter 3, the state space model is put in the form of the parameter dependent uncertain

state space systems from Chapter 2 to proceed with the stability analysis.

In this analysis, one parameter is considered uncertain at a given time. For

each parameter, several different parameter rate bounds are considered. The stability

envelope, marked by the area between the lines of a given color, is the area between

largest positive and negative variations from the nominal parameter value for which the

LMI stability criteria are found feasible. The area between the dotted red lines represents

the parameter values for quadratic stability. Table 5.1 compares the stability envelopes

obtained using the LMI criteria for a zero rate bound to results from LTI criteria.

Table 5.1: Stability Envelope Comparison for Rate Bound = 0 (t = 60 sec)

	Affine PDS Lower Bound	HO PDS Lower Bound	True Lower Bound	Affine PDS Upper Bound	HO PDS Upper Bound	True Upper Bound
Aero. Coeff.	-1	-.99	-1	1.67	1.68	1.68
Thrust	-.59	-.59	-.59	4.9	9.08	10+
Slosh Freq.	-.94	-.94	-.97	10+	10+	10+
Slosh Damp	-1.02	-1.02	-1.02	10+	10+	10+
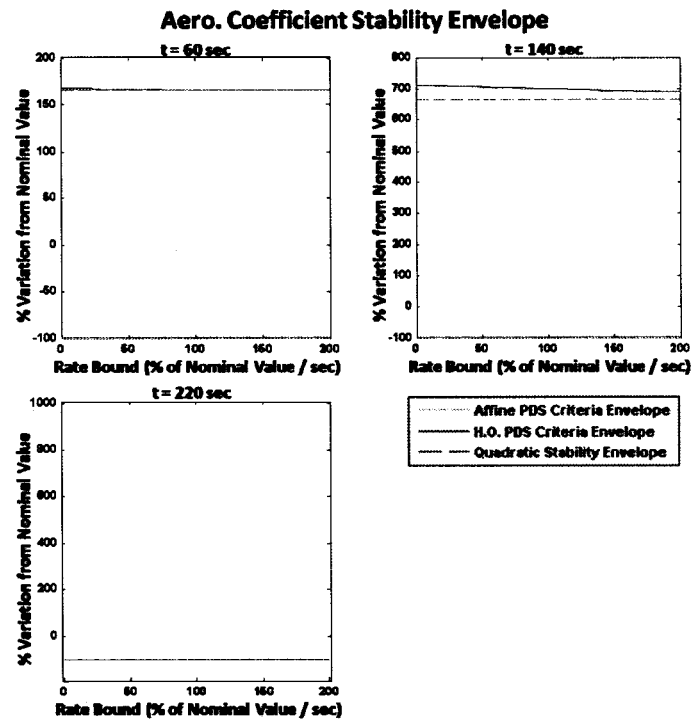
Figure 5.5: Aerodynamic Coefficient Stability Envelope

Thrust Stability Envelope

Figure 5.6: Thrust Stability Envelopes

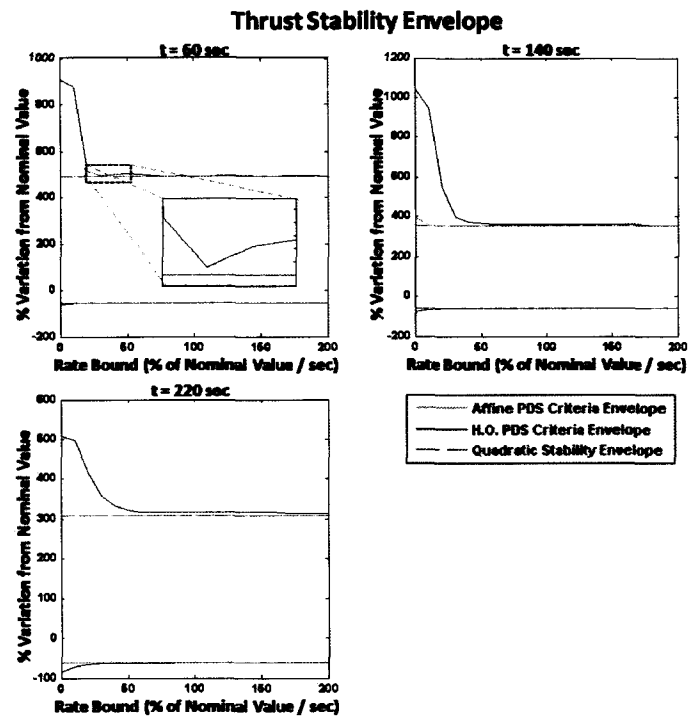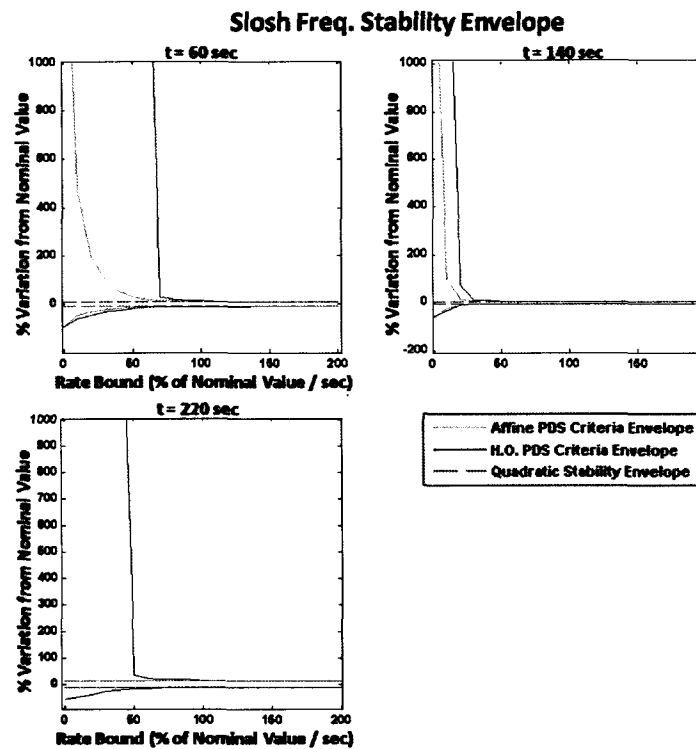**Slosh Freq. Stability Envelope**

Figure 5.7: Slosh Frequency Stability Envelopes

For all of the parameters except thrust, the time-varying stability envelopes correspond with the LTI results quite well when the parameter rates are held to zero. The thrust stability envelope, however, displays conservativeness in the LMI results. Further, the highlighted portion of Figure 5.6 shows that at 60 seconds, the stability envelope upper bound for thrust is lower at a rate bound of 30% of the nominal value per second than it is for a rate bound of 50%. Since the former, slower rate is included in the latter, it should yield a stability envelope of equal or larger size. The thrust uncertainty most likely causes conservativeness when associated with parameter dependent Lyapunov functions because the high order of magnitude typically associated with thrust causes a violation of limits placed on the norm [28] of the solutions to the feasibility problem. These limits are not currently able to be removed or increased due to limited computational abilities. By additional study, it is hoped to confirm the origin of and subsequently circumvent the computational difficulties encountered for the uncertain thrust parameter.

In this case study, the higher-order PDS model and stability criteria yields a less conservative stability envelope than the affine PDS model and LMIs for almost every uncertain parameter. This is contrary to the performance of the methods in the simple spring-mass-damper example in Chapter 3. For some of the test cases, the affine PDS stability envelope reverts immediately to the quadratic stability envelope. This trend of conservativeness is attributed to the multi-convexity constraint in the affine PDS stability criteria which applies when the system and the Lyapunov function depend on at least one of the same uncertain parameters. Due to the discrepancy in the performance of the methods for this spacecraft system, the higher-order PDS model and stability criteria are used for the remainder of the case study.

5.4 Relative Stability for a Rigid Spacecraft

As stated in Chapter 4, the LMI stability criteria can be used to determine whether or not a time-varying control system meets relative stability requirements. This is accomplished by applying a system representative of the desired margin to the system's open loop transfer function.

Knowledge of the parameter values and rates of change can be used to reduce conservativeness in testing for stability margins in a spacecraft control system. Dividing the entire timeline into smaller time intervals decreases the uncertain parameter regions that must be tested in the LMI criteria. The parameter rates of variation can be derived by analyzing the varying parameter values over time. The extreme values of the uncertain parameters' ranges and rates within a specific time interval define the parameter region for a given LMI test, as shown in Figure 5.8 for a theoretical parameter p_i.
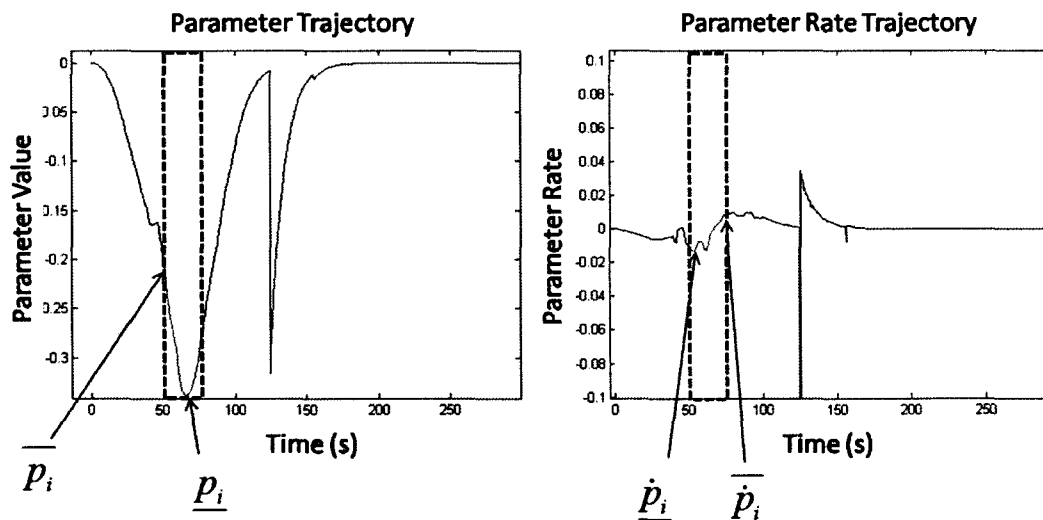

Figure 5.8: Time Interval Analysis of Parameter Trajectory

To test for gain margin in the vehicle examined in this case study, a static gain equal to the desired gain margin is added to the controller, as shown in Figure 5.9.
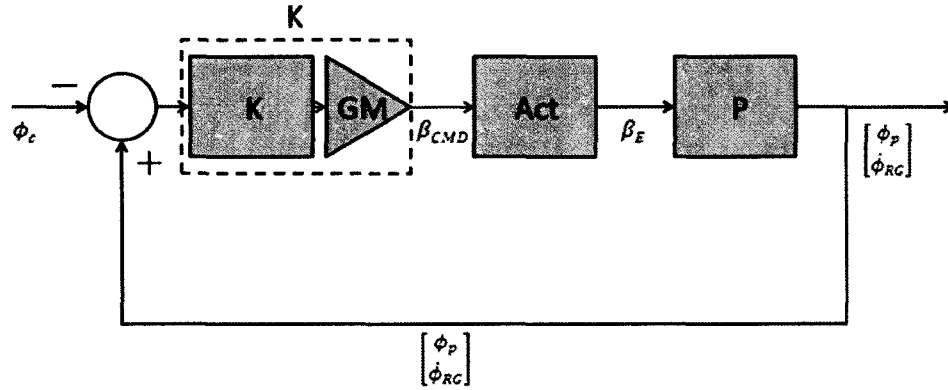

Figure 5.9: Block Diagram System with Desired Gain Margin

If the LMI criteria are found simultaneously feasible for the system in Equation 5.15 with and without the applied gain margin, the system meets the gain margin requirements for the tested operating conditions. The results in this section are based on the evaluation of the system for overlapping time intervals which are pieced together to cover longer periods of the time of flight. Therefore, the LMI criteria must be determined feasible or infeasible for the parameter rates and ranges in each interval.

A common minimum gain margin requirement in industry is $\pm 6dB$ [46], which implies stability for magnitude changes of the open loop system between

$$GM_- = 10^{\left(\frac{-6dB}{20}\right)} = .5012 \sim \frac{1}{2} \qquad (5.16)$$

and

$$GM_+ = 10^{\left(\frac{6dB}{20}\right)} = 1.995 \sim 2. \qquad (5.17)$$

As stated in Chapter 4, testing for these two margins simultaneously will determine if the system meets the design specifications.

To avoid optimistic results, phase margin testing requires that time-invariant systems be formed at the vertices of each time interval's uncertain parameter region. The frequency, ω_1, is selected as the lowest of the crossover frequencies for the smallest phase margin of each system. The phase margin is applied to the system in the form of a time delay as described in Chapter 4 and illustrated in Figure 5.11 and 5.12.
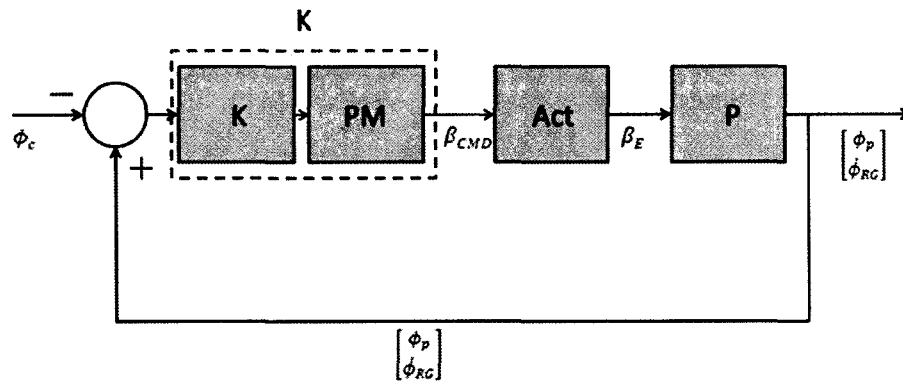

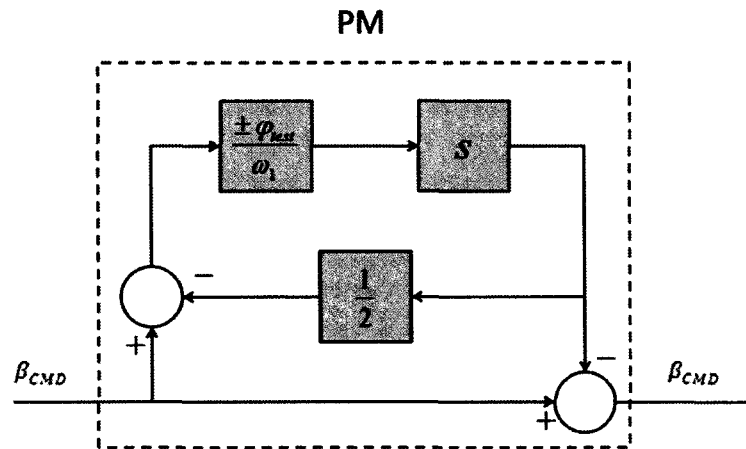Figure 5.10: Block Diagram with Desired Phase Margin Attached

Figure 5.11: First Order Padé Approximation of Desired Phase Margin Block

A common phase margin requirement for an attitude control system is

$$\varphi_{test} = \pm 30° = \pm \frac{\pi}{6} \, rad. \tag{5.18}$$

[46][47]. Since the nominal system includes a delay, it is necessary to test for positive and negative phase changes. Therefore, if the stability LMIs are found simultaneously feasible for the system in Equation 5.15 with the positive and the negative phase margin included, the original system meets phase margin requirements for the time interval tested.

In the plots that follow, a green asterisk indicates that the stability criteria are feasible for all uncertain parameter rates and ranges in the time interval. A red asterisk, indicates that the criteria were found infeasible for those parameter values. The values 0, 1, and 2 on the vertical axis correspond to quadratic, affine-quadratic (i.e. affinely parameter dependent), and biquadratic LMI stability criteria, respectively. See Section 3.3.2.3 or [11] and [39] to recall the differences between these criteria.
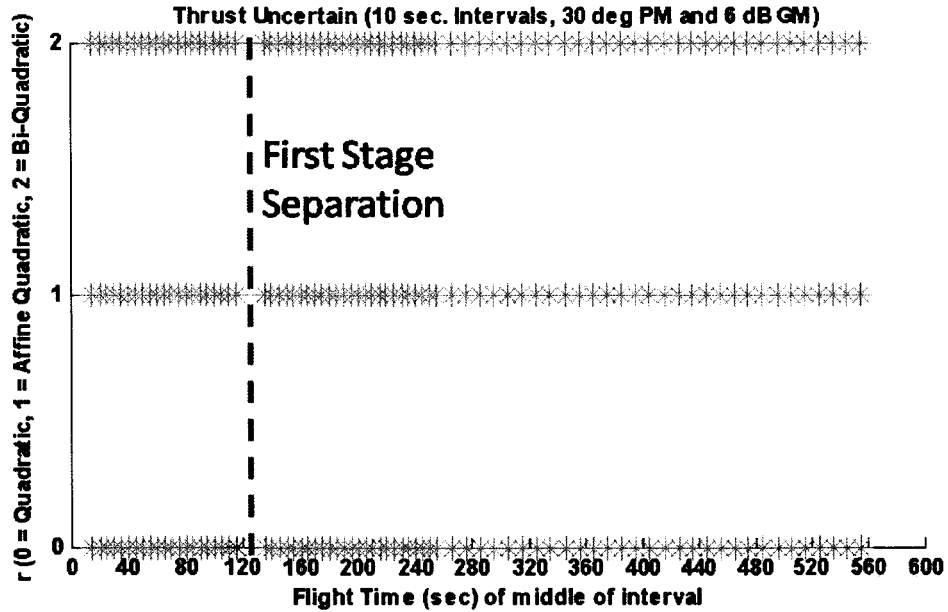

Figure 5.12: Interval Testing for Uncertain Thrust

Slosh Freq. & Damping Uncertain (10 sec. Intervals, 30 deg PM and 6 dB GM)

First Stage
Separation

r (0 = Quadratic, 1 = Affine Quadratic, 2 = Bi-Quadratic)

Flight Time (sec) of middle of interval
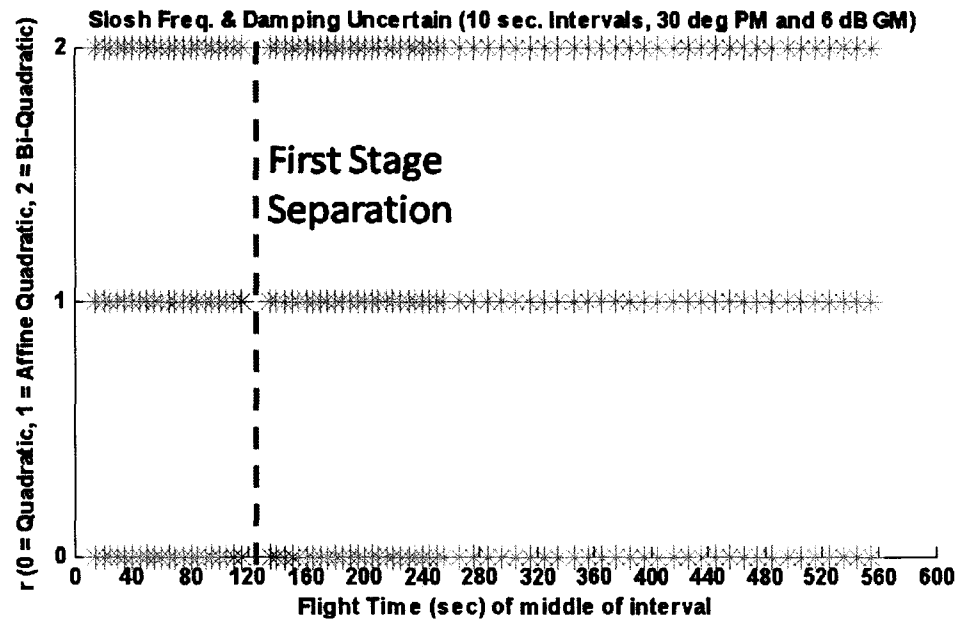
Figure 5.13: Interval Testing for Uncertain Slosh Freq. and Damping

Aero. Coeff. & Vel. Uncertain (10 sec. Intervals, 30 deg PM and 6 dB GM)

First Stage
Separation

r (0 = Quadratic, 1 = Affine Quadratic, 2 = Bi-Quadratic)

Flight Time (sec) of middle of interval
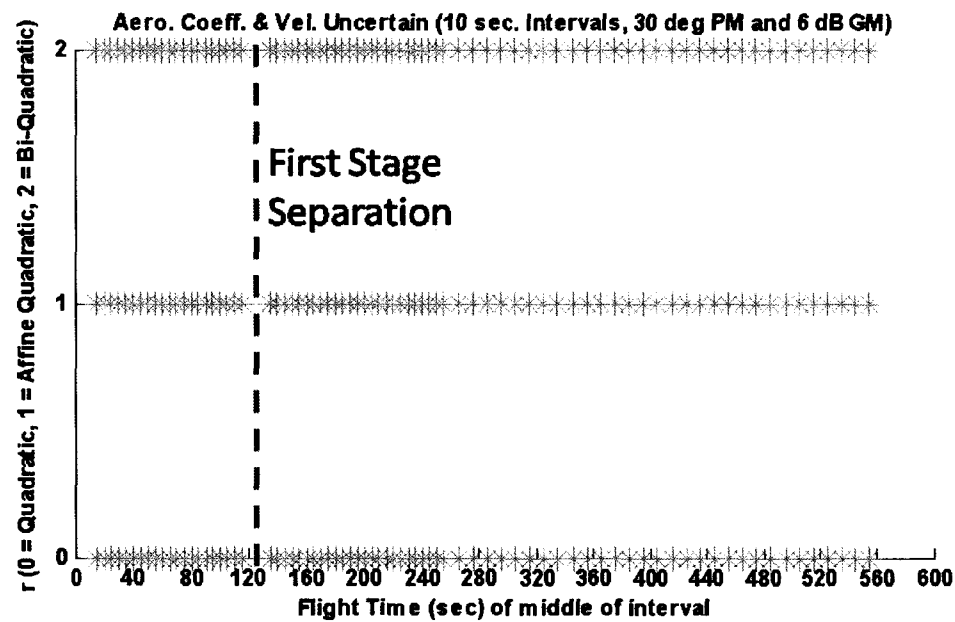
Figure 5.14: Interval Testing for Uncertain Aero Coeff. and Velocity

Note that the time interval between 120 seconds and 130 seconds into the time of

flight is left out of the analysis. For this case study, this is the interval of time during

which the first stage separates from the rest of the spacecraft. This separation features

non-linear behavior which is not captured by the system model considered in this thesis [51]. Since analyzing the separation subinterval does not offer valuable insight for this thesis, the time of flight is divided into the two intervals of time before and after separation.

According to these results, this attitude control system model possesses the required stability margins for the tested combinations of uncertain, time-varying parameters throughout the pre- and post-separation time intervals. With the exception of brief time intervals surrounding the separation subinterval, the system is found quadratically stable for most of the flight. When the quadratic stability criteria are found infeasible for the uncertain thrust or slosh characteristics, the parameter rates are slow enough for the system to be found to meet requirements by the parameter dependent Lyapunov LMI criteria. The time subintervals for which the requirements are not met can be verified with simple time-responses. For example, according to the red star in the bottom row of Figure 5.12, the system does not meet requirements for the range of thrust values on the ten second subinterval centered around t = 115 seconds if the thrust may vary arbitrarily fast. To verify this finding, a system is created with all parameters frozen at the nominal values for t = 115 seconds except for thrust. Thrust is time-varying within the range of values expected in that time interval but at faster rates. Figure 5.15 shows that at least one example of such a time-varying thrust causes the otherwise invariant system to go unstable. In the real control system, thrust varies at a bounded rate. The top row of Figure 5.12 models the system as a higher-order PDS and considers the rate bounds in the stability criteria as described in Chapter 3. According to this analysis, the system meets the robustness requirements. Therefore, parameter dependent system

models and LMI stability criteria based on biquadratic Lyapunov functions should be

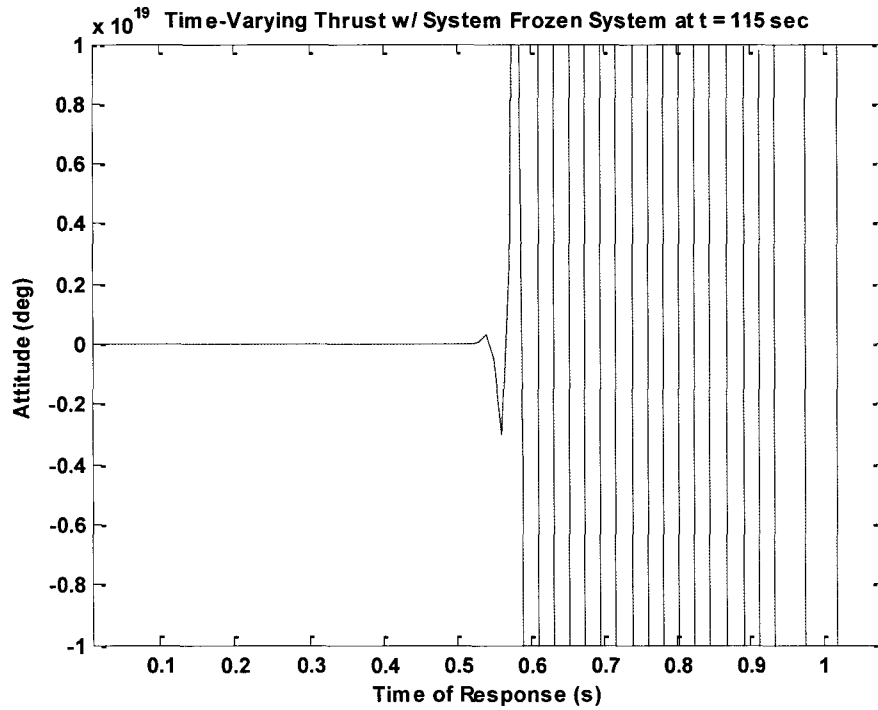used for time-varying robustness analysis of the linear control system.

Figure 5.15: Time-Response for Frozen System at t = 115 sec w/ Time-Varying Thrust

The subintervals for which the LMI stability criteria predict that the system meets

the requirements are quite difficult to validate with time responses because every possible

operating condition within the range and rate boundaries must be considered. Note that

the cases considered here feature small quantities of uncertain time-varying parameters

relative to the number of parameters that are actually time-varying on a spacecraft

system. For this reason, the analysis featured in this thesis is not intended to replace high

fidelity time-domain simulation like that presented in [3]. Instead, these results serve

only as evidence for the possibility of beneficial applications of LMI stability analysis

methods for spacecraft systems.

5.5 Stability for Full Spacecraft Dynamics

In addition to the simplified system of the previous sections, it is important to make sure the methods described in this thesis can also be applied to more complicated control system models. This section considers a higher fidelity model of the vehicle described in the case study.

In the current and following sections, the bending dynamics and filter are replaced into the control system model. This model will also include the effect of "tail-wags-dog" and "dog-wags-tail" dynamics between the plant and actuator.

Figure 5.19 portrays a block diagram of the larger system model.
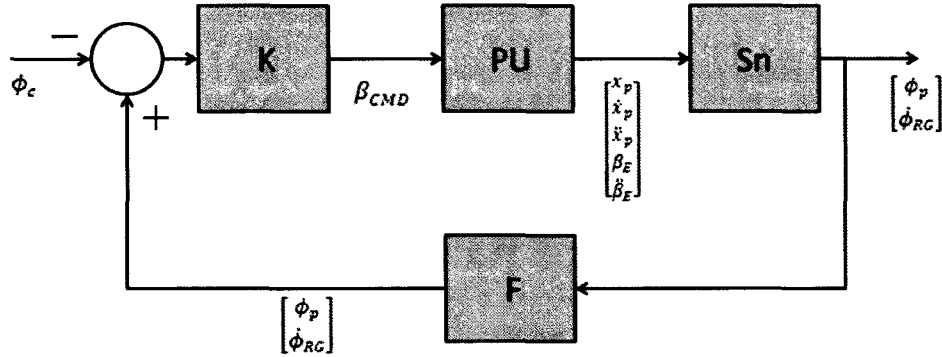
Figure 5.16: Spacecraft Attitude Control System Block Diagram

The block designated PU represents the plant and the actuator in series with the "tail-wags-dog" and "dog-wags-tail" represented as a part of the component's internal dynamics. Consider the state space models,

$$\dot{x}_{act} = A_{act}x_{act} + B_{act}y_K \qquad (5.19)$$

$$y_{act} = \begin{bmatrix} \beta_E \\ \ddot{\beta}_E \end{bmatrix} = C_{act}x_{act} + D_{act}\begin{bmatrix} \beta_{cmd} \\ T_{dwt} \end{bmatrix} \qquad (5.20)$$

and

$$\dot{x}_p = \begin{bmatrix} \dot{x}_p \\ \ddot{x}_p \end{bmatrix} = A_p(\delta)x_p + B_p(\delta)y_{act} \tag{5.21}$$

$$y_p = \begin{bmatrix} x_p \\ \dot{x}_p \\ \ddot{x}_p \\ y_{act} \end{bmatrix} = C_p(\delta)x_p + D_p y_{act}, \tag{5.22}$$

for the actuator and plant, respectively. Then, the state space system equations for the open loop plant-actuator combined system can take the form

$$\dot{x}_{pu} = A_{pu}x_{pu} + B_{pu}u_{pu} =$$

$$\begin{bmatrix} \begin{bmatrix} \dot{x}_p \\ \ddot{x}_p \end{bmatrix} \\ \dot{x}_{act} \end{bmatrix} = \begin{bmatrix} A_p(\delta) & B_p(\delta)C_{act} \\ 0 & A_{act} \end{bmatrix} x_{pu} + \begin{bmatrix} B_p(\delta)D_{act} \\ B_{act} \end{bmatrix} \begin{bmatrix} \beta_{cmd} \\ T_{dwt} \end{bmatrix} \tag{5.23}$$

$$y_{pu} = C_{pu}x_{pu} + D_{pu}u_{pu} =$$

$$\begin{bmatrix} x_p \\ \dot{x}_p \\ \ddot{x}_p \\ \beta_E \\ \ddot{\beta}_E \end{bmatrix} = [C_p(\delta) \quad D_p C_u]x_{pu} + [D_p D_u]\begin{bmatrix} \beta_{cmd} \\ T_{dwt} \end{bmatrix}. \tag{5.24}$$

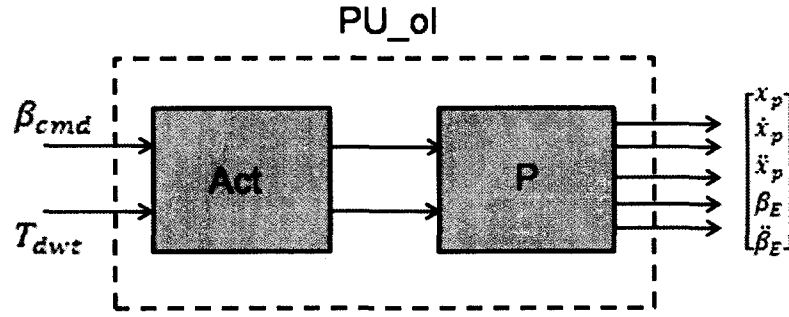This open loop system is shown in Figure 5.17.

Figure 5.17: Block Diagram of Actuator and Plant Systems

The effect of the vehicle motion on the gimbal angle described by the "dog-wags-tail" dynamics,

$$T_{dwt} = D_{dwt}y_{pu},$$ (5.25)

is included in the plant-actuator system dynamics by closing the loop. The state space system equations for the closed loop, single-input, plant-actuator system become

$$\dot{x}_{pu} = \hat{A}_{pu}x_{pu} + \hat{B}_{pu}\beta_{cmd}$$

$$= \left(A_{pu}(\delta) + B_{pu_{dwt}}(\delta)D_{dwt}\Gamma^{-1}C_{pu}(\delta)\right)x_{pu} + B_{pu_\beta}(\delta)\beta_{cmd}$$ (5.26)

$$y_{pu} = \hat{C}_{pu}x_{pu} + \hat{D}_{pu}\beta_{cmd}$$

$$= \Gamma^{-1}C_{pu}x_{pu} + D_{pu_\beta}\beta_{cmd},$$ (5.27)

where

$$\Gamma = (I - D_{pu_{dwt}}D_{dwt}).$$ (5.28)

In these equations, B_{pu_β} and D_{pu_β} represent the columns of B_{pu} and D_{pu} that correspond to β_{cmd}. Likewise, $B_{pu_{dwt}}$ and $D_{pu_{dwt}}$ represent the columns of B_{pu} and D_{pu} that

correspond to the T_{dwt} input from Figure 5.17 and Equations 5.23 and 5.24. The closed loop plant-actuator system is shown in Figure 5.18.
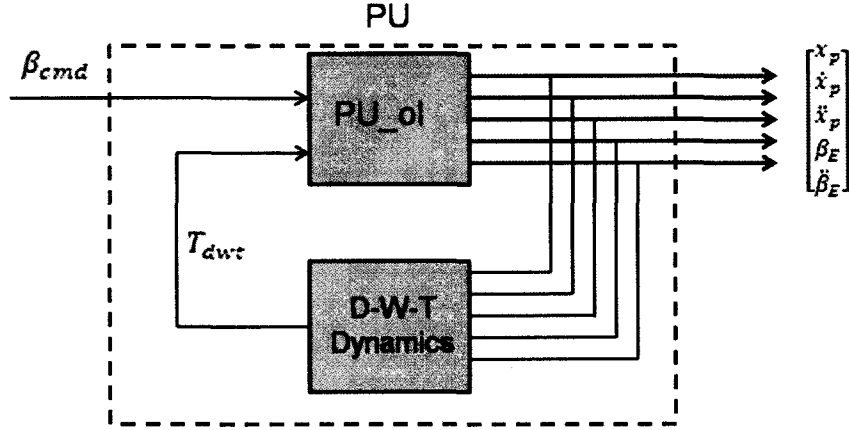
Figure 5.18: Closed Loop DWT Dynamics in Plant and Actuator

This model and the state space models,

$$y_S = \begin{bmatrix} \phi_p \\ \dot{\phi}_{RG1} \\ \dot{\phi}_{RG2} \\ \dot{\phi}_{RG3} \\ \dot{\phi}_{RGab} \end{bmatrix} = D_S y_{pu}, \tag{5.29}$$

$$\dot{x}_F = A_F x_F + B_F y_S \tag{5.30}$$

$$y_F = \begin{bmatrix} \phi_p \\ \dot{\phi}_{RG} \\ \dot{\phi}_{RGab} \end{bmatrix} = C_F x_F + D_F y_S, \tag{5.31}$$

and

$$\dot{x}_K = A_K x_K + B_K y_F \tag{5.32}$$

$$y_K = \beta_C = C_K x_K + D_K y_F, \tag{5.33}$$

for the sensor, filter, and controller, respectively, yield the overall homogeneous closed-loop control system

$$
\begin{bmatrix} \dot{x}_{pu} \\ \dot{x}_F \\ \dot{x}_K \end{bmatrix} = \begin{bmatrix} \hat{A}_{pu}(\delta) & \hat{B}_{pu}(\delta)D_K C_F & \hat{B}_{pu}(\delta)C_K \\ B_F D_S \hat{C}_{pu}(\delta) & A_F + B_F D_S \hat{D}_{pu}D_K C_F & B_F D_S \hat{D}_{pu}C_K \\ 0 & B_K C_F & A_K \end{bmatrix} \begin{bmatrix} x_{pu} \\ x_F \\ x_K \end{bmatrix}. \qquad (5.34)
$$

Notice that, even in the more complex system, the parameter dependence is restricted to the plant matrices. Using knowledge of the parameter dependence obtained from Equations 5.1 through 5.5, uncertain state space models of the system in Equation 5.34 can be formed and evaluated using LMI stability criteria.

5.6 Relative Stability for Full Spacecraft Dynamics

The testing of relative stability specifications for the higher fidelity model can be performed using the same methods as for the simplified model in Section 5.4. Parameter value and rate over time subintervals can be used to determine whether or not the gain and phase margin requirements are met over periods of the time of flight.
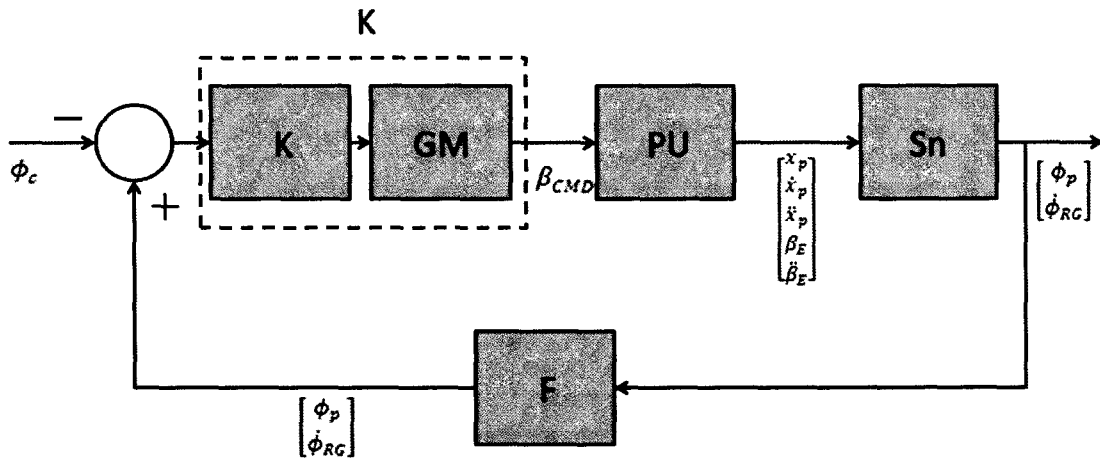
Figure 5.19: Spacecraft Attitude Control System with Gain Margin
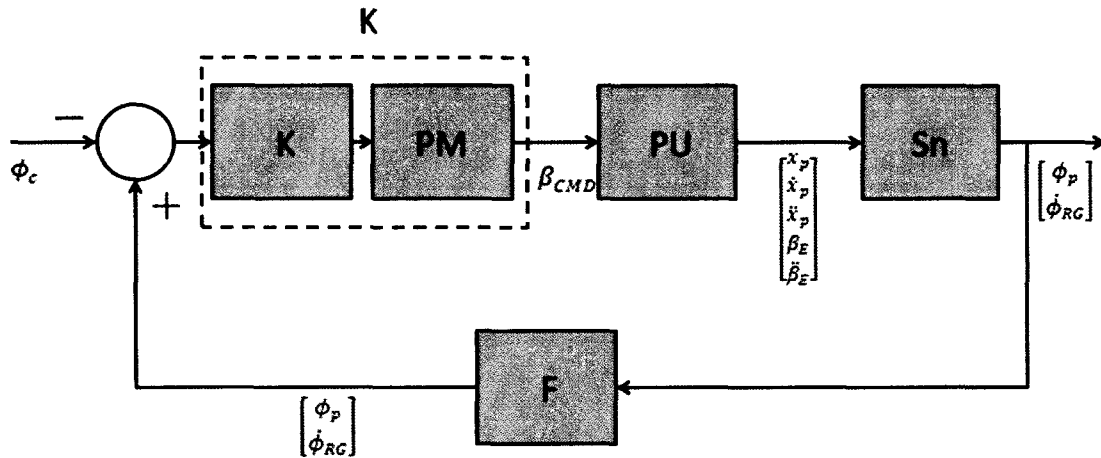
Figure 5.20: Spacecraft Attitude Control System with Phase Margin

Figures 5.19 and 5.20 display the full spacecraft attitude control system with the gain and phase margins included, respectively.

Due to limits in computational tools available for this work, the increased system size resulting from the inclusion of the bending dynamics and the filter leads to memory problems and excessive computation times. Given the right tools and sufficient time, however, the described LMI methods can provide meaningful stability analysis for time-varying linear systems like the spacecraft in this case study.

6 Closure

In this thesis, three sets of LMI stability criteria have been described. Two of these methods have been explored further in the case study to test the tools' ability to analyze the stability of an example spacecraft attitude control system model. The set of criteria pertaining to the polytopic system model has not been applied in the case study due to its inability to consider bounds on parameter rates of variations and its resulting conservative stability predictions for slowly time-varying linear systems.

In addition to using the stability criteria for stability analysis, the time-varying systems and LMI conditions have been adapted to determine whether or not required gain and phase margins are met over a range of parameter ranges and rates.

In the case study, parameter dependent Lyapunov functions and LMI stability criteria have been used to find stability envelopes, or ranges of parameter variations for which the system is stable, for several parameters. These stability envelopes have been compared to stability envelopes found using linear time-invariant stability criteria. The comparison has indicated minimal conservativeness when the uncertain parameters had rates of variation equal to zero for all tested parameters except thrust. Further, the theoretical expectation that the stability envelopes calculated with LMI criteria decrease in size as the parameters are allowed to vary more quickly has been confirmed.

Additionally, the time of flight for the case study system has been divided into overlapping time intervals. Example parameter trajectories have been consulted to obtain ranges and rates for the time-varying parameters over each interval. For several combinations of uncertain parameters, the LMI criteria have determined that the attitude

control system in the case study possessed gain and phase margins at or above the assumed minimum required levels throughout the pre- and post-separation time intervals.

The use of LMI's for time-varying stability analysis presents several interesting avenues for future research, especially in the areas of stability and robustness analysis for complicated mechanical control systems like the spacecraft from the case study.

One area where the research findings from this thesis can be readily expanded is the size and fidelity of the control system model used in the case study. Given a more specific scope, more time, and/or more computing resources, it is possible to use tools like the ones described in this thesis to analyze larger systems or systems with more and different combinations of uncertain parameters. This kind of research yields results that are more applicable to answering actual engineering design questions for aerospace systems.

Similar research with other LMI formulations may assist in finding the most efficient methods for analyzing the stability and relative stability for time-varying linear systems. For example, in [45], LMIs are formed using integral quadratic constraints based on an LFT model to analyze the stability and performance of time-varying linear systems, including those with slowly varying uncertain parameters. [27], [52], and [53] describe other LMI formulations for analyzing polynomial linear-parametrically-varying (LPV) systems. Moreover, [24] suggests that making educated choices about the parameter values in the testing regions may yield less conservative results than those obtained by using hyper-rectangular parameter regions like the ones used in this thesis.

The combination of this "small-hull" parameter modeling and the use of parameter rate information as described in this thesis may reduce conservatism even further.

The possibility for extending this research to include more kinds of uncertain systems is also interesting. In [54], LMI methods are used to design a controller for a system with saturation. Similar methods may be able to be applied to the non-linear controller described in [15] to see how they compare with other non-linear analysis methods. If this analysis yields acceptable results, the next step may be to analyze a system similar to the spacecraft in the case study without eliminating the non-linearities, like those described in [3], that have been linearized or deemed negligible in this thesis.

Bibliography

[1] Van Tassel, C. *Stability Analysis for the Ares-I Launch Vehicle*, Houston: Rice University, 2008, Master's Thesis.

[2] Jang, J., Van Tassell, C., and Bedrossian, N., "Evaluation of Ares-I Control System Robustness to Uncertain Aerodynamics and Flex Dynamics," *AIAA GN&C Conference*, Honolulu, HI, 2008, AIAA-2008-6621.

[3] Betts, K. M., Rutherford, R. C., McDuffie, J., Johnson, M.D., Jackson, M., and Hall, C. "Time Domain Simulation of the NASA Crew Launch Vehicle," AIAA *Modeling and Simulation Technologies Conference and Exhibit*, Hilton Head, SC, 2007, AIAA 2007-6621.

[4] Betts, K. M., Rutherford, R. C., McDuffie, J., Johnson, M.D., Jackson, M., and Hall, C. "Stability Analysis of the NASA ARES I Crew Launch Vehicle Control System" AIAA *Guidance, Navigation, and Control Conference and Exhibit*, Hilton Head, SC, 2007, AIAA 2007-6776.

[5] Greensite, A., *Analysis and Design of Space Vehicle Flight Control Systems*, United States: Spartan Books, 1970.

[6] Rubinstein, R., *Simulation and the Monte Carlo Method*, New York: John Wiley & Sons, 1981.

[7] Roberts, J. B. and Spanos, P.D., *Random Vibration and Statistical Linearization*. Mineola: Dover Publications, 1999.

[8] Sobol, I. M., *A Primer for the Monte Carlo Method*, Boca Raton: CRC Press, 1994.

[9] Gahinet, P., Nemirovski, A., Laub, A., and Chilali, M., *LMI Control Toolbox For Use with MATLAB*, Natick: The Math Works, Inc., 1995.

[10] Souza, C. and Trofino, A., "Bi-Quadratic Stability of Uncertain Linear Systems," *Proceedings of the 38th Conference on Decision and Control*, 1999, pp. 5016-5021.

[11] Trofino, A., "Parameter Dependent Lyapunov Functions for a Class of Uncertain Linear Systems: an LMI Approach," *Proceedings of the 38th Conference on Decision and Control*, 1999, pp. 2341-2346.

[12] Feron, E., Apkarian, P., and Gahinet, P., "Analysis and Synthesis of Robust Control Systems via Parameter-Dependent Lyapunov Functions," *IEEE Transactions on Automatic Control*, July 1996, vol. 41, pp. 1041-1046.

[13] Gahinet, P., Apkarian, P., and Chilali, M., "Affine Parameter-Dependent Lyapunov Functions and Real Parametric Uncertainty," *IEEE Transactions on Automatic Control*, March 1996, vol. 41, pp. 436-442.

[14] Frosch, J. and Vallely, D., "Saturn AS-501/ S-IC Flight Control System Design," *Journal of Spacecraft*, August 1967, vol. 4, pp. 1003-1009.

[15] Plummer, M., *Stability Analysis of a Phase Plane Control System*, Houston: Rice University, 2009, Master's Thesis.

[16] Jang, J., Hall, R., and Bedrossian, N., "Ares-I Bending Filter Design Using a Constrained Optimization Approach," *AIAA GN&C Conference*, Honolulu, HI, 2008, AIAA-2008-6289.

[17] DiStefano III, J. J., Stubberud, A. R., and Williams, I. J., *Schaum's Outline of Theory and Problems in Feedback and Control Systems*, 2nd Edition, United States : McGraw-Hill, 1990.

[18] Nise, N., *Control Systems Engineering*, 4th Edition, Pomona: John Wiley & Sons, Inc., 2004.

[19] Kamen, E. W., "Fundamentals of Linear Time-Varying Systems," *The Control Handbook*, W.S. Levine, editor, Boca Raton: CRC Press, 1996.

[20] Balas, G. J., Doyle, J. C., Glover, K., Packard, A., and Smith, R., *μ-Analysis and Synthesis Toolbox For Use with MATLAB*, Natick: The Math Works, Inc., 1995.

[21] Farag, A. and Werner, H., "Constructing Tight LFT Uncertainty Models For Robust Controller Design," *43rd IEEE Conference on Decision and Control*, Atlantis, Paradise Island, Bahamas, 2004, TuA12.2.

[22] Skogestad, S. and Postlethwaite, I., *Multivariable Feedback Control*, 2nd Edition, West Sussex: John Wiley & Sons, Ltd., 2005.

[23] Rockafellar, R. T., *Convex Analysis*, Princeton: Princeton University Press, 1970.

[24] Kumar, A. and Anderson, M., "A Comparison of LPV Modeling Techniques for Aircraft Control," *AIAA Guidance, Navigation, and Control Conference and Exhibit*, Denver, CO, 2002, AIAA 2000-4458.

[25] Pedrycz, W., editor, *Granular Computing: An Emerging Paradigm*, New York: Physica-Verlag Heidelberg, 2001.

[26] Hespanha, J., *Linear Systems Theory*, Princeton: Princeton University Press, 2009.

[27] Amato, F., "Robust Control of Linear Systems Subject to Uncertain Time Varying Parameters," *Lecture Notes in Control and Information Sciences*, vol. 325, Netherlands: Springer – Verlag Berlin HeidelBerg, 2006.

[28] Lipschutz, S. and Lipson, M. *Schaum's Outline of Linear Algebra*, 4th Edition, United States: McGraw-Hill, 2009.

[29] De La Sen, M. "Robust Stability of a Class of Linear Time-Varying Systems," *IMA Journal of Mathematical Control and Information*, vol. 19, 2002, pp. 399-418.

[30] Vidyasagar, M., *Nonlinear Systems Analysis*, 2nd Edition, Philadelphia: SIAM, 2002.

[31] Haddad, W. M. and Chellaboina, V., *Nonlinear Dynamical Systems and Control: A Lyapunov-Based Approach*, Princeton University Press: Princeton, 2008.

[32] Skelton, R. E., Iwasaki, T., and Grigoriadis, K., *A Unified Algebraic Approach to Linear Control Design*, Great Britain: Taylor & Francis Ltd, 1998.

[33] Stewart, J., *Calculus: Early Vectors*, California: Brooks/Cole, 1999.

[34] Seigler, T. and Neal, D., "Analysis of Transitional Stability for Morphing Aircraft," *Journal of Guidance, Control, and Dynamics*, vol. 32, 2009, pp. 1947-1954.

[35] Boyd, S., Ghaoui, L., Feron, E., and Balakrishnan, V., *Linear Matrix Inequalities in System and Control Theory,* Philadelphia: SIAM Books, 1994.

[36] Rizzi, A., editor, and Vichi, M., editor, *COMPSTAT: Proceedings In Computational Statistics*, Rome: Physica Verlag Heidelberg, 2006.

[37] Mahmoud, M.S., *Robust Control and Filtering for Time-Delay Systems*, New York: Marcel Dekker, 2000.

[38] Calafiore, G., Dabbene, F. editors, *Probabilistic and Randomized Methods for Design under Uncertainty.*, Germany: Springer-Verlag London Limited, 2006.

[39] Trofino, A. and de Souza, C. E., "Biquadratic Stability of Uncertain Linear Systems," *IEEE Transactions on Automatic Control*, vol. 46, August 2008, pp. 1303-1307.

[40] Kim, J. and Lyou, J., "Absolute Stability Margin in Missile Guidance Loop," *SICE-ICASE International Joint Conference 2006*, Bexco, Busan, Korea, 2006, pp. 851-855.

[41] Miotto, P., *Fixed Structure Methods for Flight Control Analysis and Automated Gain Scheduling*, Cambridge: Massachusetts Institute of Technology, 1997, Doctoral Dissertation.

[42] Hsu, H. P., *Schaum's Outline of Theory and Problems of Signals and Systems*, New York: McGraw-Hill, 1995.

[43] Baker, G. A. Jr. and Graves-Morris, P., *Encyclopedia of Mathematics and its Applications: Padé Approximants*, 2nd edition, New York: Cambridge University Press, 1996.

[44] Apkarian, P. and Adams, R., "Advanced Gain-Scheduling Techniques for Uncertain Systems," *IEEE Transactions on Control Systems Technology*, vol. 6, January 1998, pp. 21-31.

[45] Siersma, M., Van der Weerd, R., and Bennani, S. "Robustness Analysis of a Gain-Scheduled Flight Control System Using Integral Quadratic Constraints," *AIAA Guidance, Navigation, and Control Conference and Exhibit*, Denver, CO, 2000, AIAA-2000-4460.

[46] Hall, C. E. and Panossian, H. V., "X-33 Attitude Control Using the XRS-2200 Linear Aerospike Engine," 35th *AIAA/ASME/SAE/ASEE Joint Propulsion Conference and Exhibit*, Los Angeles, CA, 1999, AIAA 99-2936.

[47] Y Naruo, Y Inatani, Y Morita, S Nakai & H Mori, "Throttling Dynamic Response of LH2 Rocket Engine for Vertical Landing Rocket Vehicle", *7th International Space Conference of Pacific Basin Societies*, Nagasaki, Japan, 1997, AASx 97-421.

[48] Hiret, A., Duc, G., Friang, J. P., and Farret, D., "Linear-Parameter-Varying/Loop-Shaping H_∞ Synthesis for a Missile Autopilot," *Journal of Guidance, Control, and Dynamics*, vol. 24, 2001, pp. 879-886.

[49] Symens, W., Van Brussel, H., Swevers, J. and Paijmans, B. "Gain-Scheduling of Machine Tools with Varying Structural Flexibilities," *Active Vibration Control and Smart Structures, Proceedings of ISMA 2004*, 2004, pp. 301-310.

[50] Nichkawde, C., Harish P. M., and Ananthkrishnan, N., "Stability Analysis of a Multibody System Model for Coupled Slosh–Vehicle Dynamics," *Journal of Sound and Vibration*, vol. 275, 2004, pp. 1069-1083.

[51] Rao B. N., Jeyakumar D., Biswas K. K., Swaminathan S., and Janardhana E., "Rigid body separation dynamics for space launch vehicles," *Aeronautical Journal, vol. 110, 2006, pp. 289-302.*

[52] Coutinho, D., Souza, C., and Trofino, A. "Stability Analysis of Implicit Polynomial Systems," *IEEE Transactions on Automatic Control*, vol. 54, 2009, pp. 1012-1018.

[53] Wu, F. and Prajna, S. "A New Solution to Polynomial LPV System Analysis and Synthesis," *Proceedings of the ACC 2004*, 2004, pp. 1-6.

[54] Grigoriadis, K. M. and Wu. F., "Actuator Saturation Control via Linear Parameter-Varying Control Methods," *Actuator Saturation Control*, Kapila, V. and Grigoriadis K.M. editors, New York: Marcel Dekker, 2003 pp. 273-98.